Full-Duplex Small-Cell Networks: A Physical-Layer Security Perspective

Ayda Babaei, *Student Member, IEEE*, Abdol Hamid Aghvami, *Fellow, IEEE*
Arman Shojaeifard, *Member, IEEE*, Kai-Kit Wong, *Fellow, IEEE*,

***Abstract*—We provide a theoretical study of physical (PHY)-layer security performance in full-duplex (FD) small-cell networks. Here, the multi-antenna base stations (BSs) and user equipments (UEs) follow from the homogeneous Poisson point process (PPP)-based abstraction model. To facilitate FD communications, we take into account (i) successive interference cancellation (SIC) capability at the UE side via guard regions of arbitrary radii, and (ii) residual self-interference (SI) at the BS side using Rician fading distribution with arbitrary statistics. We investigate the small-cell network PHY-layer security performance in the presence of a Poisson field of eavesdroppers (EDs), under the different scenarios of passive and colluding eavesdropping. Considering linear zero-forcing (ZF) beamforming, we characterize the downlink (DL) and uplink (UL) ergodic secrecy rates and derive closed-form expressions for the different useful and interference signals statistics. In certain special cases of interest, we apply non-linear curve-fitting techniques to large sets of (exact) theoretical data in order to obtain closed-form approximations for the different ergodic rates and ergodic secrecy rates under consideration. Our findings indicate that the FD functionality, in addition to enhancing the spectral efficiency (SE), can significantly improve the PHY-layer security performance, especially with the aid of multi-antenna communications and interference cancellation schemes.**

***Index Terms*—Full-duplex small-cells, multi-antenna communications, ergodic secrecy rate, applied probability theory, non-linear curve-fitting, system-level analysis.**

I. Introduction

Legacy cellular networks have been designed and dimensioned according to a complete separation of the transmit and receive functionalities (what is known as half-duplex (HD) operation). Specifically, the transceiving of wireless signals, from the base station (BS) to the user equipment (UE) in the downlink (DL), and from the UE to the BS in the uplink (UL), are either separated orthogonally in time or frequency domain; two prominent examples include time-division duplex (TDD) and frequency-division duplex (FDD) systems. A major motivation behind this design and dimensioning approach has been to bypass the extra interference which arises from the bi-directional wireless functionality, namely, residual self-interference (SI) at each FD transceiver, and mutual interference (MI) between the DL and the UL modes of communications [3], [4].

Full-duplex (FD) operation, that is joint transmission and reception of wireless signals at the same time and frequency, has emerged as a disruptive technology for improving the spectral efficiency (SE) performance in wireless systems [5], [6]. Recently, there have been major advances in the family of techniques used to combat SI directly in FD mode, including any combination of analog, digital, and spatial domain cancellation [7]–[9]. In addition, the MI, a main limiting factor in large-scale adoption of FD functionality, can be effectively tackled through applying interference management techniques such as successive interference cancellation (SIC) [10], [11]. With the aid of advanced techniques for tackling SI and MI, it has been shown that significant FD versus HD SE gains can be achieved in cellular networks [12]–[15]. The adoption of FD functionality is considered particularly attractive for dense small-cell BS deployment in the fifth generation (5G) cellular networks and beyond [16].

Physical (PHY)-layer security is a de facto requirement for the safeguarding of wireless systems [17]. It is quantified by the difference in the useful and eavesdropping channel capacities, what is known as secrecy rate [18]. This topic has received a great deal of attention in recent years, including the study of PHY-layer security in the context of relays [19]–[21], cognitive radios [22], [23], heterogeneous networks [24], wireless information and power transfer [25], and cloud radio access networks [26]. Given that the locations of the eavesdroppers (EDs) are in most cases not known to the network, they can be modeled using stochastic processes. There already exists a very rich literature on the design, modeling, and analysis of large-scale wireless systems with random ED locations, see, e.g., [27]–[30]. More recently, the impact of randomly-located cooperating (a.k.a., colluding) EDs has also been investigated in [31].

The emergence of FD operation provides a new paradigm concerning all aspects of wireless system design, including PHY-layer security performance. This topic has been investigated in the recent literature (see, e.g., [32] and the references therein for a survey). In [33], the authors proposed a new solution for improving the PHY-layer security performance using FD transceivers which perform joint reception and jamming. The work in [33], as well as other related papers such as [34]–[36], consider a deterministic single-cell setup. In addition, the recent works in [37] and [38] study the PHY-layer security performance in the context of FD-enabled wireless ad hoc networks. To the best of our knowledge, the fundamental

A. Babaei and A. H. Aghvami are with the Centre for Telecommunications Research (CTR), Department of Informatics, King's College London, Strand, London WC2R 2LS, United Kingdom. (e-mail: ayda.babaei@kcl.ac.uk; hamid.aghvami@kcl.ac.uk).

A. Shojaeifard and K-K. Wong are with the Communications and Information Systems Group (CISG), Department of Electronic and Electrical Engineering, University College London, Torrington Place, London WC1E 7JE, United Kingdom. (e-mail: a.shojaeifard@ucl.ac.uk; kai-kit.wong@ucl.ac.uk).

This work was supported by the United Kingdom Engineering and Physical Sciences Research Council (EPSRC) under Grant no. EP/N008219/1.

Parts of this work were presented at the IEEE PIMRC 2017, Montreal, QC, Canada [1] and the IEEE VTC-Spring 2018, Porto, Portugal [2].

PHY-layer security performance in large-scale FD small-cell networks is currently not well understood.

In this work, we aim to bridge the gap by devising a unified theoretical framework for the study of ergodic secrecy rate performance in FD small-cell networks where the locations of the passive or colluding EDs are unknown. The main technical contributions of this work can be summarized as follows:

- We study the PHY-layer security performance of large-scale FD multi-user MIMO cellular networks under the homogeneous Poisson point process (PPP)-based abstraction model of BSs, UEs, and EDs, with different scenarios of passive and colluding eavesdropping.
- The residual SI channels are characterized using the Rician distribution with arbitrary statistics which allows for the capturing of the PHY-layer security performance under different SI cancellation capabilities.
- We consider the generalized case where the UEs may be capable of performing SIC through imposing guard regions of arbitrary radii when modeling the UE-UE interference.
- By leveraging on the tools from stochastic geometry theory, we derive explicit expressions for the DL and UL ergodic secrecy rates, with the statistics of the different useful and interference signals given in closed-form.
- In certain special scenarios of interest, we utilize non-linear curve-fitting techniques in order to provide closed-form approximations for the different ergodic rates and ergodic secrecy rates under consideration.

With the aid of the proposed analytical model, as well as Monte-Carlo (MC) simulations, we draw network design insights. Our findings illustrate that significant FD versus HD PHY-layer security performance gains can be achieved, particularly through adopting advanced interference cancellation schemes for tackling SI and MI. Conditioned on the system experiencing secrecy non-outage, the relative FD versus HD PHY-layer security performance gain (i) increases in the number of small-cell BS transmit/receive antennas, (ii) increases in the EDs' spatial deployment densities, and (iii) decreases in the number of DL/UL UEs served per resource block. The results also highlight that the underlying advantages of FD over HD functionality in terms of ergodic secrecy rates can be greater in the case of colluding versus passive eavesdropping, due to the increased interference levels affecting the individual EDs' SINRs in FD mode.

Organization: The remainder of this work is organized as follows. The large-scale small-cell network model and operation is described in Section II. The theoretical study of the PHY-layer security performance is given in Section III. Numerical examples are provided in Section IV, and finally, conclusions are drawn in Section V.

Notation: $\boldsymbol{X}$ is a matrix; $\boldsymbol{x}$ is a vector; T, $\dagger$, and $+$ are the transpose, Hermitian, and pseudo-inverse operations; $\mathbb{E}_x[.]$ is the expectation; $\Pr[.]$ is the probability; $\mathcal{F}_x[.]$ is the cumulative distribution function (CDF); $\mathcal{P}_x[.]$ is the probability density function (PDF); $\mathcal{L}_x[.]$ is the Laplace transform (LT) function; $|x|$ is the modulus; $\|\boldsymbol{x}\|$ is the Euclidean norm; $[x]^+ = \max(x, 0)$ is the Ramp function; $\mathbf{I}_{(.)}$ is the identity matrix; $\mathcal{CN}(\mu, \nu^2)$ is the circularly-symmetric complex Gaussian distribution with mean μ and variance ν^2; $\Gamma(.)$ and $\Gamma(.,.)$ are the Gamma and incomplete (upper) Gamma functions; $\mathcal{G}(\kappa, \theta)$ is the Gamma distribution with shape parameter κ and scale parameter θ; and ${}_2F_1(.,.;.;.)$ is the Gauss hypergeometric function, respectively.

II. System Description

A. Network Topology

Consider a large-scale small-cell network where the FD BSs and HD UL UEs are deployed based on homogeneous PPPs ϕ_d and ϕ_u with spatial densities λ_d and λ_u, respectively. Each FD small-cell BS, equipped with N_d transmit and N_u receive antennas ($N_d + N_u$ radio-frequency chains in total), is considered to simultaneously serve K_d DL and K_u UL HD single-antenna UEs per resource block. Note that the assumption of HD UEs is made due to the inherent restrictions of the legacy devices [39], otherwise, the framework can be readily extended to the case of FD UEs [40]. The locations of the EDs are generally not known to the network, therefore in this work, they are modeled according to a homogeneous PPP ϕ_e with spatial density λ_e [26], [27]. Moreover, we consider the different scenarios where the (single-antenna) EDs are operating independently and cooperatively [31]. Note that with obvious adjustments, the HD system, where the DL and UL occur over different resource blocks, can be described.

B. Cellular Association

By invoking the Slivnyak's theorem [41], we perform the DL analysis for a typical HD UE o considered to be located at the center. Let $l \in \phi_d$, $k \in \phi_u$, and $e \in \phi_e$ denote the locations of the BS l, UL UE k, and ED e, respectively. We consider the cellular association strategy based on the maximum received signal-to-interference-plus-noise ratio (SINR) [42]. Here, this is equivalent to cellular association based on the shortest transmitter-receiver distances [43]. Mathematically, the tagged BS of the reference DL UE o satisfies $b = \arg\min(r_{l,o}), l \in \phi_d$, where $r_{l,o} = \|l - o\|$ denotes the Euclidean distance. The UL analysis, on the other hand, is carried out at the tagged BS b with respect to the signal of an arbitrary HD UL UE i. It should be noted that due to the cellular association procedure, the scheduled UEs locations are inherently correlated [44]. Here, conditioning on the spatial constraints, we assume that the set of scheduled UEs in the UL follows from a stationary PPP [45], [46]. Further, we consider the most malicious EDs in the DL and UL, respectively denoted with v and c, which receive the strongest SINRs [19]. In the case of collusion, we consider the cooperative EDs are capable of optimally combining their eavesdropping signals [47], [48].

C. Fading Channel Model

Let p_d and p_u denote the (per-user) BS and UE transmit powers, respectively. The DL channel gains from the BS l at the UE k and ED e are $\boldsymbol{g}_{l,k} \in \mathcal{C}^{1\cdot N_d}$ and $\boldsymbol{g}_{l,e} \in \mathcal{C}^{1\cdot N_d}$, respectively. Further, we denote the UL channel gains from the UE k at the BS l and ED e using $\boldsymbol{h}_{k,l} \in \mathcal{C}^{N_u\cdot 1}$ and $h_{k,e}$, respectively. The cross-mode channel gains from the

BS l at the BS b, and from the UE k at the UE o are represented using $\boldsymbol{H}_{l,b} \in \mathcal{C}^{N_u \cdot N_d}$ and $g_{k,o}$, respectively. In addition, the residual SI channel gain at the BS b is denoted with $\boldsymbol{H}_{b,b} \in \mathcal{C}^{N_u \cdot N_d}$. The residual SI channels are Rician distributed with independent and identically distributed (i.i.d.) $\mathcal{CN}(\mu, \nu^2)$ coefficients [49]. All other channels are considered to be Rayleigh distributed with i.i.d. elements drawn from $\mathcal{CN}(0,1)$. In addition, we utilize the unbounded path-loss model with exponent $\alpha > 2$.

D. Beamfomring Design

In this work, we employ linear zero-forcing (ZF) beamforming for suppressing intra-cell interference in both DL and UL directions of communications [50]. Let $\boldsymbol{G}_l = [\boldsymbol{g}_{l,j}^T]_{1 \le j \le K_d}^T \in \mathcal{C}^{K_d \cdot N_d}$ denote the collective DL channels from the BS l to its K_d DL UEs. At the BS l, the linear ZF precoding matrix $\boldsymbol{V}_l = [\boldsymbol{v}_{l,j}]_{1 \le j \le K_d} \in \mathcal{C}^{N_d \cdot K_d}$, $\mathbb{E}[\|\boldsymbol{v}_{l,j}\|^2] = 1$, is selected equal to the normalized columns of $\boldsymbol{G}_l^+ = \boldsymbol{G}_l^\dagger (\boldsymbol{G}_l \boldsymbol{G}_l^\dagger)^{-1} \in \mathcal{C}^{N_d \cdot K_d}$. Moreover, let $\boldsymbol{H}_l = [\boldsymbol{h}_{j,l}]_{1 \le j \le K_u} \in \mathcal{C}^{N_u \cdot K_u}$ represent the collective UL channels at the BS l from its K_u scheduled UL UEs. At the BS l, the linear postcoding ZF matrix $\boldsymbol{W}_l = [\boldsymbol{w}_{j,l}^T]_{1 \le j \le K_u}^T \in \mathcal{C}^{K_u \cdot N_u}$, $\mathbb{E}[\|\boldsymbol{w}_{j,l}\|^2] = 1$, is selected equal to the normalized rows of $\boldsymbol{H}_l^+ = (\boldsymbol{H}_l^\dagger \boldsymbol{H}_l)^{-1} \boldsymbol{H}_l^\dagger \in \mathcal{C}^{K_u \cdot N_u}$.

E. SINR Formulation

The received SINR (considering FD BSs) in the DL at the UE o under linear ZF precoding is given by

$$\gamma_o^{\text{FD}} = \frac{X_o}{I_o^{d,d} + I_o^{u,d} + \sigma_o^2} \tag{1}$$

where $X_o = p_d |\boldsymbol{g}_{b,o} \boldsymbol{v}_{b,o}|^2 r_{b,o}^{-\alpha}$ is the intended received signal power (from the serving BS), $I_o^{d,d} = \sum_{l \in \phi_d \setminus \{b\}} p_d \|\boldsymbol{g}_{l,o} \boldsymbol{V}_l\|^2 r_{l,o}^{-\alpha}$ is the inter-cell interference (from the transmitting BSs), $I_o^{u,d} = \sum_{k \in \phi_u} p_u |h_{k,o}|^2 r_{k,o}^{-\alpha}$ is the cross-mode interference (from the transmitting UEs), and σ_o^2 is the noise variance. The linear ZF precoding vector $\boldsymbol{v}_{b,o}$ is selected in the direction of the projection of $\boldsymbol{g}_{b,o}$ on the $(N_d - K_d + 1)$-dimensional nullspace spanned by the multi-user interference. Hence, the distribution of the intended channel power gain is given by $G_{b,o} = |\boldsymbol{g}_{b,o} \boldsymbol{v}_{b,o}|^2 \sim \mathcal{G}(N_d - K_d + 1, 1)$ [51], [52]. With the assumption that the other BSs precoding matrices have independent columns, the channel power gain from each interfering BS is interpreted as the aggregation of multiple separate beams from the projection of $\boldsymbol{g}_{l,o}$ onto the one-dimensional precoding vectors. Based on this assumption, the inter-cell interference channel power gain distribution is given by $G_{l,o} = \|\boldsymbol{g}_{l,o} \boldsymbol{V}_l\|^2 \sim \mathcal{G}(K_d, 1)$. Moreover, the cross-mode interference (from the single-antenna UEs) channel power gain distribution is given by $H_{k,o} = |h_{k,o}|^2 \sim \mathcal{G}(1,1)$.

The received SINR (considering FD BSs) in the UL at the BS b with respect to the signal from an arbitrary UL UE i under linear ZF postcoding is given by

$$\gamma_i^{\text{FD}} = \frac{X_i}{I_i^{u,u} + I_i^{d,u} + I_i^i + \sigma_i^2} \tag{2}$$

where $X_i = p_u |\boldsymbol{w}_{i,b}^T \boldsymbol{h}_{i,b}|^2 r_{i,b}^{-\alpha}$ is the intended received signal power (from the reference UE), $I_i^{u,u} = \sum_{k \in \hat{\phi}_u} p_u |\boldsymbol{w}_{i,b}^T \boldsymbol{h}_{k,b}|^2 r_{k,b}^{-\alpha}$, with $\hat{\phi}_u$ denoting the set of outer-cell scheduled UL UEs, is the inter-cell interference (from the transmitting UEs), $I_i^{d,u} = \sum_{l \in \phi_d \setminus \{b\}} p_d \|\boldsymbol{w}_{i,b}^T \boldsymbol{G}_{l,b} \boldsymbol{V}_l\|^2 r_{l,b}^{-\alpha}$ is the cross-mode interference (from the transmitting BSs), $I_i^i = p_b \|\boldsymbol{w}_{i,b}^T \boldsymbol{G}_{b,b} \boldsymbol{V}_b\|^2$ is the residual self-interference (from the bi-directional operation), and σ_i^2 is the noise variance. Considering linear ZF postcoding, the intended channel power gain distribution is given by $H_{i,b} = |\boldsymbol{w}_{i,b}^T \boldsymbol{h}_{i,b}|^2 \sim \mathcal{G}(N_u - K_u + 1, 1)$. Moreover, the inter-cell interference (from the single-antenna UEs) channel power gain distribution is given by $H_{k,b} = |\boldsymbol{w}_{i,b}^T \boldsymbol{h}_{k,b}|^2 \sim \mathcal{G}(1,1)$. By invoking the assumption of independent (column-wise) outer-cell precoding matrices, the cross-mode interference (from transmitting BSs) channel power gain distribution is given by $G_{l,b} = \|\boldsymbol{w}_{i,b}^T \boldsymbol{G}_{l,b} \boldsymbol{V}_l\|^2 \sim \mathcal{G}(K_d, 1)$. Furthermore, the residual SI channel power gain over the multi-user multiple-input multiple-output (MIMO) Rician fading channel can be approximated as $G_{b,b} = \|\boldsymbol{w}_{i,b}^T \boldsymbol{G}_{b,b} \boldsymbol{V}_b\|^2 \sim \mathcal{G}(\kappa, \theta)$ where (3) and (4) [49], as shown at the bottom of this page.

The received SINR (considering FD BSs) in the DL at the most malicious passive and colluding ED v are respectively given by

$$\gamma_v^{\text{FD}} = \max_{e \in \phi_e} \left(\frac{X_e}{I_e^{d,d} + I_e^{u,d} + \sigma_e^2} \right) \tag{5}$$

and

$$\gamma_v^{\text{FD}} = \sum_{e \in \phi_e} \left(\frac{X_e}{I_e^{d,d} + I_e^{u,d} + \sigma_e^2} \right) \tag{6}$$

where $X_e = p_d \|\boldsymbol{g}_{b,e} \boldsymbol{v}_{b,e}\|^2 r_{b,e}^{-\alpha}$ is the intended received signal (from the serving BS), $I_e^{d,d} = \sum_{l \in \phi_d} p_d \|\boldsymbol{g}_{l,e} \boldsymbol{V}_l\|^2 r_{l,e}^{-\alpha}$ is the inter-cell interference (from the transmitting BSs), $I_e^{u,d} = \sum_{k \in \phi_u} p_u \ |h_{k,e}|^2 r_{k,e}^{-\alpha}$ is the cross-mode interference (from the transmitting UEs), and σ_e^2 is the noise variance. The channel power gain distributions are given by $G_{b,e} = \|\boldsymbol{g}_{b,e} \boldsymbol{v}_{b,e}\|^2 \sim \mathcal{G}(1,1)$, $G_{l,e} = \|\boldsymbol{g}_{l,e} \boldsymbol{V}_l\|^2 \sim \mathcal{G}(K_d, 1)$, and

$$\kappa \triangleq \frac{K_d (N_u + 1)(N_d - K_d + 2) \left(\mu^2 + \nu^2\right)^2}{\left(2N_u N_d + \frac{K_d (N_d - K_d + 2)}{N_u + 1} (N_u N_d - N_u - N_d - 1)\right) \mu^4 + (N_u + 1)(N_d + 1) \nu^2 \left(2\mu^2 + \nu^2\right)} \tag{3}$$

$$\theta \triangleq \frac{\left(2N_u N_d + \frac{K_d (N_d - K_d + 2)}{(N_d + 1)} (N_u N_d - N_u - N_d - 1)\right) \mu^4 + (N_u + 1)(N_d + 1) \nu^2 \left(2\mu^2 + \nu^2\right)}{(N_u + 1)(N_d - K_d + 2)(\mu^2 + \nu^2)} \tag{4}$$

$$C_o^{\text{FD}} = \frac{4\pi\lambda_d}{\ln(2)} \int_0^{\infty} \int_0^{\infty} \frac{1}{1+\gamma} \left(\sum_{n=0}^{N_d-K_d} \left\{ \frac{(-s)^n}{n!} \frac{\mathrm{d}^n}{\mathrm{d}s^n} \exp\left(-s\sigma_o^2\right) \mathscr{L}_{I_o^{d,d}}[s] \mathscr{L}_{I_o^{u,d}}[s] \right\}_{s=\frac{\gamma r^\alpha}{p_d}} \right) \mathrm{d}\gamma r \exp\left(-\pi\lambda_d r^2\right) \mathrm{d}r \quad (9)$$

$$C_o^{\text{HD}} = \frac{2\pi\lambda_d}{\ln(2)} \int_0^{\infty} \int_0^{\infty} \frac{1}{1+\gamma} \left(\sum_{n=0}^{N_d-K_d} \left\{ \frac{(-s)^n}{n!} \frac{\mathrm{d}^n}{\mathrm{d}s^n} \exp\left(-s\sigma_o^2\right) \mathscr{L}_{I_o^{d,d}}[s] \right\}_{s=\frac{\gamma r^\alpha}{p_d}} \right) \mathrm{d}\gamma r \exp\left(-\pi\lambda_d r^2\right) \mathrm{d}r \quad (10)$$

$$\mathscr{L}_{I_o^{d,d}}[s] = \exp\left(-\pi\lambda_d r^2 \left({}_2F_1\left(K_d, -\frac{2}{\alpha}; 1-\frac{2}{\alpha}; -\frac{sp_d}{r^\alpha} \right) - 1 \right) \right) \quad (11)$$

$$\mathscr{L}_{I_o^{u,d}}[s] = \exp\left(-\pi K_u \lambda_d \varepsilon^2 \left({}_2F_1\left(1, -\frac{2}{\alpha}; 1-\frac{2}{\alpha}; -\frac{sp_u}{\varepsilon^\alpha} \right) - 1 \right) \right) \quad (12)$$

$H_{k,e} = |h_{k,e}|^2 \sim \mathcal{G}(1,1)$.

The received SINR (considering FD BSs) in the UL at the most malicious passive and colluding ED c are respectively given by

$$\gamma_c^{\text{FD}} = \max_{e\in\phi_e} \left(\frac{X_e}{I_e^{u,u} + I_e^{d,u} + \sigma_e^2} \right) \quad (7)$$

and

$$\gamma_c^{\text{FD}} = \sum_{e\in\phi_e} \left(\frac{X_e}{I_e^{u,u} + I_e^{d,u} + \sigma_e^2} \right) \quad (8)$$

where $X_e = p_u |h_{o,e}|^2 r_{o,e}^{-\alpha}$ is the intended received signal (from the reference UE), $I_e^{u,u} = \sum_{k\in\phi_u} p_u |h_{k,e}|^2 r_{k,e}^{-\alpha}$ is the inter-cell interference (from the transmitting UEs), $I_e^{d,u} = \sum_{l\in\phi_d} p_d \ \|\boldsymbol{g}_{l,e}\boldsymbol{V}_l\|^2 r_{l,e}^{-\alpha}$ is the cross-mode interference (from the transmitting BSs), and σ_e^2 is the noise variance. The channel power gain distributions are given by $H_{o,e} = |h_{o,e}|^2 \sim \mathcal{G}(1,1)$, $H_{k,e} = |h_{k,e}|^2 \sim \mathcal{G}(1,1)$, and $G_{l,e} = \|\boldsymbol{g}_{l,e}\boldsymbol{V}_l\|^2 \sim \mathcal{G}(K_d,1)$.

Note that the EDs' SINR expressions in this work correspond to the case where the EDs have no information regarding the codebook of UEs and BSs. However, the analysis can be modified to capture other scenarios (e.g., by removing certain interference terms from the EDs' SINRs) [53].

III. Analysis

In this section, we study the PHY-layer security performance in FD small-cell networks under both scenarios of passive and colluding eavesdropping. Note that the ergodic rates (in b/s/Hz) of the reference DL and UL UEs, o and i, over two resource blocks, are given by $C_o^{\text{FD}} = 2\mathbb{E}[\log_2(1+\gamma_o^{\text{FD}})]$ and $C_i^{\text{FD}} = 2\mathbb{E}[\log_2(1+\gamma_i^{\text{FD}})]$ in FD mode, and $C_o^{\text{HD}} = \mathbb{E}[\log_2(1+\gamma_o^{\text{HD}})]$ and $C_i^{\text{HD}} = \mathbb{E}[\log_2(1+\gamma_i^{\text{HD}})]$ in HD mode, respectively. Similarly, the ergodic rates (in b/s/Hz) of the most malicious DL and UL EDs, v and c, over two resource blocks, are given by $C_v^{\text{FD}} = 2\mathbb{E}[\log_2(1+\gamma_v^{\text{FD}})]$ and $C_c^{\text{FD}} = 2\mathbb{E}[\log_2(1+\gamma_c^{\text{FD}})]$ in FD mode, and $C_v^{\text{HD}} = \mathbb{E}[\log_2(1+\gamma_v^{\text{HD}})]$ and $C_c^{\text{HD}} = \mathbb{E}[\log_2(1+\gamma_c^{\text{HD}})]$ in HD mode, respectively.

Remark 1. By invoking the Jensen's inequality, $\mathbb{E}[\max(X,Y)\} \geq \max\{\mathbb{E}\{X\}, \mathbb{E}\{Y\}]$, the bounded DL and UL ergodic secrecy rates (considering FD BSs) are respectively given by $S_o^{\text{FD}} = [C_o^{\text{FD}} - C_v^{\text{FD}}]^+$ and $S_i^{\text{FD}} = [C_i^{\text{FD}} - C_c^{\text{FD}}]^+$. Similarly, in the case of HD operation, the bounded DL and UL ergodic secrecy rates are respectively given by $S_o^{\text{HD}} = [C_o^{\text{HD}} - C_v^{\text{HD}}]^+$ and $S_i^{\text{HD}} = [C_i^{\text{HD}} - C_c^{\text{HD}}]^+$.

A. User Equipments

We proceed by deriving explicit expressions for the DL and UL UEs ergodic rates under linear ZF beamforming. Note that the DL MI is characterized considering the UEs may be capable of performing SIC. In order to capture performance for general cases, we consider an exclusion region of radius ε when modeling the UE-UE interference [54].

Theorem 1. The DL ergodic rates (in b/s/Hz) of the useful UE o in the FD and HD small-cell networks over two resource blocks are given by (9) and (10) where (11) and (12), as shown at the top of this page.

Proof: See Appendix A.

Remark 2. The guard region radius ε in the MI expression in (12) can be set by design or through measurements based on the SIC capability at the UE side. In particular, $\varepsilon = 0$ corresponds to the worst-case without SIC capability.

Theorem 2. The UL ergodic rates (in b/s/Hz) of the useful UE i in the FD and HD small-cell networks over two resource blocks are given by (13) and (14) where (15), (16), and (17), as shown at the top of the next page.

Proof: See Appendix B.

Remark 3. The Rician fading distribution parameters μ and ν in the residual SI expression in (17) can be tuned by design or measurements to capture the SI cancellation capability at the BS side. For example, $\nu = 0$ and $\mu = 0$ correspond to perfect SI removal and non line-of-sight (NLOS) SI, respectively.

Remark 4. The derivatives of the interfering terms LT functions required for the calculation of the ergodic rates in the *Theorems 1-2*, which arise as a result of multi-antenna communications, can be readily computed through applying the Faà di Bruno's formula [55].

B. Passive Eavesdroppers

Next, we derive explicit expressions for the ergodic rates of the most malicious passive EDs in the DL and UL. Note

$$C_i^{\text{FD}} = \frac{4\pi\lambda_d}{\ln(2)} \int_0^\infty \int_0^\infty \frac{1}{1+\gamma} \left(\sum_{n=0}^{N_u-K_u} \left\{ \frac{(-s)^n}{n!} \frac{\mathrm{d}^n}{\mathrm{d}s^n} \exp\left(-s\sigma_i^2\right) \mathscr{L}_{I_i^{u,u}}[s] \mathscr{L}_{I_i^{d,u}}[s] \mathscr{L}_{I_i^{i}}[s] \right\}_{s=\frac{\gamma r^\alpha}{p_u}} \right) \mathrm{d}\gamma r \exp\left(-\pi\lambda_d r^2\right) \mathrm{d}r \tag{13}$$

$$C_i^{\text{HD}} = \frac{2\pi\lambda_d}{\ln(2)} \int_0^\infty \int_0^\infty \frac{1}{1+\gamma} \left(\sum_{n=0}^{N_u-K_u} \left\{ \frac{(-s)^n}{n!} \frac{\mathrm{d}^n}{\mathrm{d}s^n} \exp\left(-s\sigma_i^2\right) \mathscr{L}_{I_i^{u,u}}[s] \right\}_{s=\frac{\gamma r^\alpha}{p_u}} \right) \mathrm{d}\gamma r \exp\left(-\pi\lambda_d r^2\right) \mathrm{d}r \tag{14}$$

$$\mathscr{L}_{I_i^{u,u}}[s] = \exp\left(-\pi K_u \lambda_d r^2 \left({}_2F_1\left(1, -\frac{2}{\alpha}; 1-\frac{2}{\alpha}; -\frac{sp_u}{r^\alpha}\right) - 1 \right) \right) \tag{15}$$

$$\mathscr{L}_{I_i^{d,u}}[s] = \exp\left(-\pi\lambda_d \left(sp_d\right)^{\frac{2}{\alpha}} \frac{\Gamma\left(1-\frac{2}{\alpha}\right)\Gamma\left(K_d+\frac{2}{\alpha}\right)}{\Gamma(K_d)} \right) \tag{16}$$

$$\mathscr{L}_{I_i^{i}}[s] = \left(1+sp_d\theta\right)^{-\kappa} \tag{17}$$

that in this case the EDs act independently (do not exchange information).

Theorem 3. The DL ergodic rates (in b/s/Hz) of the most malicious passive ED v in the FD and HD small-cell networks over two resource blocks are given by (18) and (19) where (20) and (21), as shown at the bottom of this page.

Proof: See Appendix C.

Theorem 4. The UL ergodic rates (in b/s/Hz) of the most malicious passive ED c in the FD and HD small-cell networks over two resource blocks are given by (22) and (23) where (24) and (25), as shown at the bottom of this page.

Proof: See Appendix D.

C. Colluding Eavesdroppers

The ergodic rates of the most malicious colluding EDs in the DL and UL are derived next. The cooperating EDs in this case form a distributed antenna system [47], [48]. Note

$$C_v^{\text{FD}} = \frac{2}{\ln(2)} \int_0^\infty \frac{1}{1+\gamma} \left(1 - \exp\left(-2\pi\lambda_e \int_0^\infty \left[\exp\left(-s\sigma_v^2\right) \mathscr{L}_{I_v^{d,d}}[s] \mathscr{L}_{I_v^{u,d}}[s] \right]_{s=\frac{\gamma r^\alpha}{p_d}} r \, \mathrm{d}r \right) \right) \mathrm{d}\gamma \tag{18}$$

$$C_v^{\text{HD}} = \frac{1}{\ln(2)} \int_0^\infty \frac{1}{1+\gamma} \left(1 - \exp\left(-2\pi\lambda_e \int_0^\infty \left[\exp\left(-s\sigma_v^2\right) \mathscr{L}_{I_v^{d,d}}[s] \right]_{s=\frac{\gamma r^\alpha}{p_d}} r \, \mathrm{d}r \right) \right) \mathrm{d}\gamma \tag{19}$$

$$\mathscr{L}_{I_v^{d,d}}[s] = \exp\left(-\pi\lambda_d \left(sp_d\right)^{\frac{2}{\alpha}} \frac{\Gamma\left(1-\frac{2}{\alpha}\right)\Gamma\left(K_d+\frac{2}{\alpha}\right)}{\Gamma(K_d)} \right) \tag{20}$$

$$\mathscr{L}_{I_v^{u,d}}[s] = \exp\left(-\pi K_u \lambda_d \left(sp_u\right)^{\frac{2}{\alpha}} \Gamma\left(1-\frac{2}{\alpha}\right)\Gamma\left(1+\frac{2}{\alpha}\right) \right) \tag{21}$$

$$C_c^{\text{FD}} = \frac{2}{\ln(2)} \int_0^\infty \frac{1}{1+\gamma} \left(1 - \exp\left(-2\pi\lambda_e \int_0^\infty \left\{ \exp\left(-s\sigma_c^2\right) \mathscr{L}_{I_c^{u,u}}[s] \mathscr{L}_{I_c^{d,u}}[s] \right\}_{s=\frac{\gamma r^\alpha}{p_u}} r \, \mathrm{d}r \right) \right) \mathrm{d}\gamma \tag{22}$$

$$C_c^{\text{HD}} = \frac{1}{\ln(2)} \int_0^\infty \frac{1}{1+\gamma} \left(1 - \exp\left(-2\pi\lambda_e \int_0^\infty \left\{ \exp\left(-s\sigma_c^2\right) \mathscr{L}_{I_c^{u,u}}[s] \right\}_{s=\frac{\gamma r^\alpha}{p_u}} r \, \mathrm{d}r \right) \right) \mathrm{d}\gamma \tag{23}$$

$$\mathscr{L}_{I_c^{u,u}}[s] = \exp\left(-\pi K_u \lambda_d \left(sp_u\right)^{\frac{2}{\alpha}} \Gamma\left(1-\frac{2}{\alpha}\right)\Gamma\left(1+\frac{2}{\alpha}\right) \right) \tag{24}$$

$$\mathscr{L}_{I_c^{d,u}}[s] = \exp\left(-\pi\lambda_d \left(sp_d\right)^{\frac{2}{\alpha}} \frac{\Gamma\left(1-\frac{2}{\alpha}\right)\Gamma\left(K_d+\frac{2}{\alpha}\right)}{\Gamma(K_d)} \right) \tag{25}$$

$$C_v^{\text{FD}} \leq \frac{4\pi\lambda_e p_d}{\ln(2)\gamma(1+\gamma)} \int_0^{\infty} \int_{r_0}^{\infty} r^{1-\alpha} \int_0^{\infty} \exp\left(-s\sigma_v^2\right) \mathscr{L}_{I_v^{d,d}}[s] \mathscr{L}_{I_v^{u,d}}[s] \, \mathrm{d}s \, \mathrm{d}r \, \mathrm{d}\gamma \tag{26}$$

$$C_v^{\text{HD}} \leq \frac{2\pi\lambda_e p_d}{\ln(2)\gamma(1+\gamma)} \int_0^{\infty} \int_{r_0}^{\infty} r^{1-\alpha} \int_0^{\infty} \exp\left(-s\sigma_v^2\right) \mathscr{L}_{I_v^{d,d}}[s] \, \mathrm{d}s \, \mathrm{d}r \, \mathrm{d}\gamma \tag{27}$$

$$C_c^{\text{FD}} \leq \frac{4\pi\lambda_e p_u}{\ln(2)\gamma(1+\gamma)} \int_0^{\infty} \int_{r_0}^{\infty} r^{1-\alpha} \int_0^{\infty} \exp\left(-s\sigma_c^2\right) \mathscr{L}_{I_c^{u,u}}[s] \mathscr{L}_{I_c^{d,u}}[s] \, \mathrm{d}s \, \mathrm{d}r \, \mathrm{d}\gamma \tag{28}$$

$$C_c^{\text{HD}} \leq \frac{2\pi\lambda_e p_u}{\ln(2)\gamma(1+\gamma)} \int_0^{\infty} \int_{r_0}^{\infty} r^{1-\alpha} \int_0^{\infty} \exp\left(-s\sigma_c^2\right) \mathscr{L}_{I_c^{u,u}}[s] \, \mathrm{d}s \, \mathrm{d}r \, \mathrm{d}\gamma \tag{29}$$

that most previous studies of randomly-located colluding EDs such as [31] are carried out for single-cell HD systems, where the EDs do not experience any interference. In the case of multi-cell FD systems with randomly-located colluding EDs, the analysis becomes significantly more challenging as one needs to account for the impact of MI in both the DL and the UL.

Theorem 5. The bounded DL ergodic rates (in b/s/Hz) of the most malicious colluding ED v in the FD and HD small-cell networks over two resource blocks are given by (26) and (27), as shown at the top of this page.

Proof: See Appendix E.

Theorem 6. The bounded UL ergodic rates (in b/s/Hz) of the most malicious colluding ED c in the FD and HD small-cell networks over two resource blocks are given by (28) and (29), as shown at the top of this page.

Proof: The proof follows from a similar approach to that in Appendix E.

Remark 5. The parameter r_0 in the colluding EDs ergodic rate expressions from *Theorems 5-6* represents the guard region distance required to satisfy the secrecy non-outage condition.

The expressions developed in *Theorems 1-6* can be readily used to obtain the different SEs required in the calculation of the PHY-layer security performance via two-fold integral computations. This is in line with the state-of-the-art results on stochastic geometry-based SE analysis of large-scale wireless networks in the literature [53]. Although there is no well-known method to simplify these SE expressions further, the proposed theoretical framework provides significant advantages in terms of computational complexity versus the Monte-Carlo simulations.

D. Special Cases

As previously highlighted, the SE expressions do not admit closed-forms. In what follows, we apply non-linear curve-fitting techniques to large sets of (exact) theoretical data in order to obtain some explicit closed-form approximations for the different ergodic rates and ergodic secrecy rates under consideration. We accordingly provide goodness of fit measurements in terms of R-Squared (R^2) and estimated variance (Var).

The following results are obtained for the special case where each multi-antenna small-cell BS serves a single UE per resource block in each DL/UL direction. This assumption is made for the sake of simplifying the non-linear curve-fitting operation. However, it should be noted that the single-user MIMO transmission technology is widely employed for FD small-cell BS deployment in the literature [15].

Corollary 1. Consider the special case with $N_d = N_u = N$, $K_d = K_u = 1$, $p_d = p_u$, $\alpha = 4$, $\sigma_d^2 = \sigma_u^2 = 0$. The DL ergodic rates (in b/s/Hz) of the useful UE o in the FD (with different SIC capabilities) and HD small-cell networks over two resource blocks are approximated by

$$C_o^{\text{FD}} \approx 2.78 \log\left(1 + 1.55N\right), \\ (\text{w/ SIC}, R^2 \approx 0.\dot{9}, \text{Var} \approx 2.00 \times 10^{-3}) \tag{30}$$

$$C_o^{\text{FD}} \approx 2.33 \log\left(1 + 1.3N\right), \\ (\text{w/o SIC}, R^2 \approx 0.\dot{9}, \text{Var} \approx 6.41 \times 10^{-3}) \tag{31}$$

$$C_o^{\text{HD}} \approx 1.43 \log\left(1 + 3.4N\right), \\ (R^2 \approx 0.\dot{9}, \text{Var} \approx 2.65 \times 10^{-4}). \tag{32}$$

Remark 6. The results from *Corollary 1* indicate that a significant gain in the FD DL ergodic rate can be achieved through reducing the MI level using SIC.

Corollary 2. Consider the special case with $N_d = N_u = N$, $K_d = K_u = 1$, $p_d = p_u$, $\alpha = 4$, $\sigma_d^2 = \sigma_u^2 = 0$. The UL ergodic rates (in b/s/Hz) of the useful UE i in the FD (with different residual SI) and HD small-cell networks over two resource blocks are approximated by

$$C_i^{\text{FD}} \approx 2.33 \log\left(1 + 1.3N\right), \\ (\text{w/o SI}, R^2 \approx 0.\dot{9}, \text{Var} \approx 6.41 \times 10^{-3}) \tag{33}$$

$$C_i^{\text{FD}} \approx 2.31 \log\left(1 + 1.3N\right), \\ (\text{w/ NLOS SI}, R^2 \approx 0.\dot{9}, \text{Var} \approx 6.59 \times 10^{-3}) \tag{34}$$

$$C_i^{\text{HD}} \approx 1.43 \log\left(1 + 3.4N\right), \\ (R^2 \approx 0.\dot{9}, \text{Var} \approx 2.65 \times 10^{-4}). \tag{35}$$

Remark 7. We observe based on the results from *Corollary 2* that the FD UL ergodic rate performance is largely limited by the MI as there is only a small difference in performance between the different perfect SI cancellation and NLOS SI cases.

Corollary 3. Consider the special case with $N_d = N_u = N$,

$K_d = K_u = 1$, $p_d = p_u$, $\alpha = 4$, $\sigma_d^2 = \sigma_u^2 = 0$. The DL ergodic rates (in b/s/Hz) of the most malicious passive ED v and UL ergodic rates (in b/s/HZ) of the most malicious passive ED c in the FD and HD small-cell networks over two resource blocks are approximated by

$$C_v^{\text{FD}} = C_c^{\text{FD}} \approx 5\log\left(1 + 0.55\lambda_e\right), \\ (R^2 \approx 0.\dot{9},\ \text{variance} \approx 5.31 \times 10^{-5}) \tag{36}$$

$$C_v^{\text{HD}} = C_c^{\text{HD}} \approx 3\log\left(1 + 0.9\lambda_e\right), \\ (R^2 \approx 0.\dot{9},\ \text{variance} \approx 2.85 \times 10^{-5}). \tag{37}$$

Remark 8. The results from *Corollary 3* indicate that in the case of passive EDs, the ergodic rate of the most malicious ED increases only logarithmically in the EDs' spatial density.

Corollary 4. Consider the special case with $K_d = K_u = 1$, $p_d = p_u$, $\alpha = 4$, $\sigma_d^2 = \sigma_u^2 = 0$. The DL ergodic rates (in b/s/Hz) of the most malicious colluding ED v and the UL ergodic rates (in b/s/HZ) of the most malicious colluding ED c in the FD and HD small-cell networks over two resource blocks are approximated by

$$C_v^{\text{FD}} = C_c^{\text{FD}} \approx 42\frac{\lambda_e}{r_0^2}, \\ (R^2 \approx 0.\dot{9},\ \text{variance} \approx 7.40 \times 10^{-4}) \tag{38}$$

$$C_v^{\text{HD}} = C_c^{\text{HD}} \approx 84\frac{\lambda_e}{r_0^2}, \\ (R^2 \approx 0.\dot{9},\ \text{variance} \approx 2.70 \times 10^{-4}). \tag{39}$$

Remark 9. We observe based on the results from *Corollary 4.* that in the case of colluding EDs, the ergodic rate of the most malicious colluding ED increases linearly in the EDs' spatial density.

Note that the logarithmic versus linear behavior of the most malicious ED ergodic rate in the EDs' spatial density under passive (Remark 8) and colluding (Remark 9) eavesdropping can be attributed to their corresponding SINR formulation (i.e., $\max(.)$ versus $\sum(.)$ functions).

Corollary 5. Consider the special case with $N_d = N_u = N$, $K_d = K_u = 1$, $p_d = p_u$, $\alpha = 4$, $\sigma_d^2 = \sigma_u^2 = 0$. The DL ergodic secrecy rate (in b/s/Hz) of the useful UE o with respect to the most malicious passive ED v in the FD (with different SIC capabilities) and HD small-cell networks over two resource blocks are approximated by

$$S_o^{\text{FD}} = \left[2.55\log\left(1 + 2N\right) - 2.1\lambda_e\right]^+, \\ (\text{w/ SIC}, R^2 \approx 0.\dot{9}, \text{Var} \approx 1.40 \times 10^{-2}) \tag{40}$$

$$S_o^{\text{FD}} = \left[2\log\left(1 + 2N\right) - 2.1\lambda_e\right]^+, \\ (\text{w/o SIC}, R^2 \approx 0.\dot{9}, \text{Var} \approx 1.47 \times 10^{-2}) \tag{41}$$

$$S_o^{\text{HD}} = \left[1.4\log\left(1 + 3.6N\right) - 2.1\lambda_e\right]^+, \\ (R^2 \approx 0.\dot{9}, \text{Var} \approx 1.16 \times 10^{-2}). \tag{42}$$

Corollary 6. Consider the special case with $N_d = N_u = N$, $K_d = K_u = 1$, $p_d = p_u$, $\alpha = 4$, $\sigma_d^2 = \sigma_u^2 = 0$. The UL ergodic secrecy rate (in b/s/Hz) of the useful UE i with respect to the most malicious passive ED c in the FD (with different residual SI) and HD small-cell networks over two resource blocks are approximated by

$$S_i^{\text{FD}} = \left[2\log\left(1 + 2N\right) - 2.1\lambda_e\right]^+, \\ (\text{w/o SI}, R^2 \approx 0.\dot{9}, \text{Var} \approx 1.34 \times 10^{-2}) \tag{43}$$

$$S_i^{\text{FD}} = \left[1.94\log\left(1 + 2.2N\right) - 2.1\lambda_e\right]^+, \\ (\text{w/ NLOS SI}, R^2 \approx 0.\dot{9}, \text{Var} \approx 1.47 \times 10^{-2}) \tag{44}$$

$$S_i^{\text{HD}} = \left[1.4\log\left(1 + 3.6N\right) - 2.1\lambda_e\right]^+, \\ (R^2 \approx 0.\dot{9}, \text{Var} \approx 1.16 \times 10^{-2}). \tag{45}$$

Corollary 7. Consider the special case with $N_d = N_u = N$, $K_d = K_u = 1$, $p_d = p_u$, $\alpha = 4$, $\sigma_d^2 = \sigma_u^2 = 0$. The DL ergodic secrecy rate (in b/s/Hz) of the useful UE o with respect to the most malicious colluding ED v in the FD (with different SIC capabilities) and HD small-cell networks over two resource blocks are approximated by

$$S_o^{\text{FD}} = \left[2.5\log\left(1 + 2.2N\right) - 42\frac{\lambda_e}{r_0^2}\right]^+, \\ (\text{w/ SIC}, R^2 \approx 0.\dot{9}, \text{Var} \approx 6.40 \times 10^{-2}) \tag{46}$$

$$S_o^{\text{FD}} = \left[1.9\log\left(1 + 2.5N\right) - 42\frac{\lambda_e}{r_0^2}\right]^+, \\ (\text{w/o SIC}, R^2 \approx 0.\dot{9}, \text{Var} \approx 6.41 \times 10^{-2}) \tag{47}$$

$$S_o^{\text{HD}} = \left[1.4\log(1 + 3.6N) - 84\frac{\lambda_e}{r_0^2}\right]^+, \\ (R^2 \approx 0.\dot{9}, \text{Var} \approx 8.25 \times 10^{-2}). \tag{48}$$

Corollary 8. Consider the special case with $N_d = N_u = N$, $K_d = K_u = 1$, $p_d = p_u$, $\alpha = 4$, $\sigma_d^2 = \sigma_u^2 = 0$. The UL ergodic secrecy rate (in b/s/Hz) of the useful UE i with respect to the most malicious colluding ED c in the FD (with different residual SI) and HD small-cell networks over two resource blocks are approximated by

$$S_i^{\text{FD}} = \left[1.9\log\left(1 + 2.5N\right) - 42\frac{\lambda_e}{r_0^2}\right]^+, \\ (\text{w/o SI}, R^2 \approx 0.\dot{9}, \text{Var} \approx 6.41 \times 10^{-2}) \tag{49}$$

$$S_i^{\text{FD}} = \left[1.9\log\left(1 + 2.45N\right) - 42\frac{\lambda_e}{r_0^2}\right]^+, \\ (\text{w/ NLOS SI}, R^2 \approx 0.\dot{9}, \text{Var} \approx 6.44 \times 10^{-2}) \tag{50}$$

$$S_i^{\text{HD}} = \left[1.4\log(1 + 3.6N) - 84\frac{\lambda_e}{r_0^2}\right]^+, \\ (R^2 \approx 0.\dot{9}, \text{Var} \approx 8.25 \times 10^{-2}). \tag{51}$$

Remark 10. The results from *Corollaries 5-8* indicate that the DL and UL FD (w/o SI and w/ NLOS SI) over HD ergodic secrecy rate gains under both passive and colluding eavesdropping are always greater or equal to one (with $N \geq 1$ and $\lambda_e \geq 0$) - in other words, the FD operation always achieves an improved or equivalent PHY-layer security performance versus the HD counterpart. Whilst the system experiences secrecy non-outage, increasing the number of small-cell BS antennas ($N \to +\infty$) always enhances the DL and UL FD over HD ergodic secrecy rate gains. Further, the corresponding impact of the EDs' spatial density can be described as follows. As $\lambda_e \to 0$ (no eavesdropping), the DL and UL FD over HD

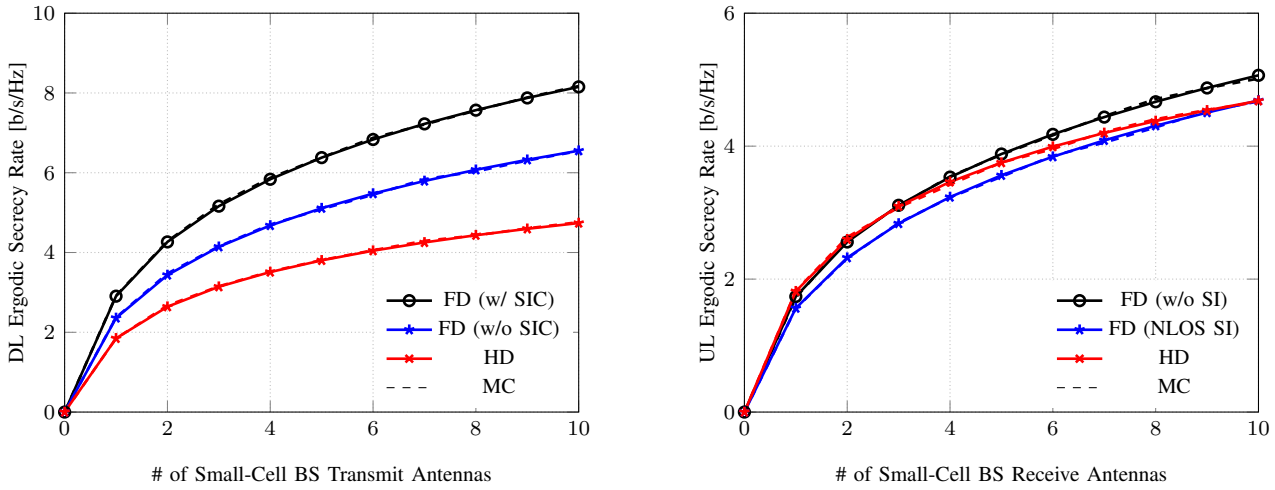

Fig. 1. Impact of the number of BS transmit/receive antennas on the small-cell network PHY-layer security performance in the presence of a Poisson field of passive EDs. System parameters are: $\lambda_d = \frac{4}{\pi}$ km^{-2}, $\lambda_u = K_u \lambda_d$ km^{-2}, $\lambda_e = \frac{\lambda_d}{10}$ km^{-2}, $K_d = K_u = 1$, $p_d = 23$ dBm, $p_u = 20$ dBm, $W = 10$ MHz, $\sigma_o^2 = \sigma_v^2 = \sigma_i^2 = \sigma_c^2 = -170$ dBm/Hz, $\alpha = 4$.

ergodic secrecy rate gains tend to the DL and UL FD over HD ergodic rate gains. Increasing λ_e from zero to λ_e^* continuously enhances the DL and UL FD over HD ergodic secrecy rate gains, where λ_e^* represents the critical point where the system experiences secrecy outage. In the limit $\lambda_e \to +\infty$, such that $\lambda_e \geq \lambda_e^*$, the DL and UL FD over HD ergodic secrecy rate gains tend to one. Note that the value of λ_e^* depends on the interference cancellation capabilities as well as the number of small-cell BS transmit/receive antennas.

In order to demonstrate the validity of the approximate expressions derived within *Corollaries 1-8* versus the (exact) theoretical data, we provide some numerical examples in Appendix F.

IV. Numerical Results

In this section, we provide several numerical examples in order to assess the PHY-layer security performance of FD and HD small-cell networks in the presence of a Poisson field of EDs. The spatial density of the small-cell BSs is set to be $\lambda^{(d)} = \frac{4}{\pi}$ per km^2. The (per-user) BS and UE transmit powers are kept fixed at $p_d = 23$ dBm and $p_u = 20$ dBm, respectively. The noise spectral density at all receivers is -170 dBm/Hz and the total system bandwidth is $W = 10$ MHz. The MC simulations are obtained from 20 k trials in a circular region of radius 10 km. Note that all results correspond to the per-user ergodic secrecy performance over two resource blocks. In the FD small-cell network, the DL and UL run simultaneously, whereas in the HD small-cell network, the DL and UL occur over different resource blocks. Furthermore, in the FD system, we take into account different interference cancellation schemes. In particular, in the DL, we consider the cases with and without SIC capability at the UE side. Moreover, in the UL, we capture the performance under different perfect SI cancellation and NLOS residual SI with a variance of -55 dB [3].

A. Impact of the Number of Base Station Antennas

1) Passive Eavesdroppers: We study the impact of the number of small-cell BS transmit and receive antennas on the small-cell network DL and UL PHY-layer security performance under a Poisson field of passive EDs in Fig. 1. It can be observed that in all cases, the ergodic secrecy rate always increases in the number of antennas. This is due to the improved array gain from multi-antenna communications, and hence, stronger useful signal power, whilst the interference level remains the same. Furthermore, the FD over HD small-cell network PHY-layer security performance gain always increases in the number of antennas. In point of fact, even with SIC capability and perfect SI suppression, only negligible FD versus HD improvements in ergodic secrecy performance can be achieved when the small-cell BSs are equipped with a few antennas. This trend highlights the essential role of MIMO in harnessing the full potential of FD technology through enhancing the system robustness against the increased interference level versus that in the HD operation [56], [57]. The presence of significant residual SI (e.g., variance > -30 dB), would typically result in secrecy outage (even when the number of antennas is relatively large). The current SI cancellation capabilities can achieve orders of magnitude greater cancellation (e.g., in the range $60 - 100$ dB [9]), hence, the FD operation is certainly feasible. It is important to note that in such cases the impact of residual SI becomes negligible compared to the MI [15], [40]. It may be useful to note that to achieve higher FD versus HD PHY-layer security performance gains in the UL, the transmit power of the small-cell BSs should be reduced. It can be observed that the MC simulations confirm the validity of our findings in *Theorems 1-4*.

2) Colluding Eavesdroppers: Next, the impact of the number of small-cell BS transmit and receive antennas on the small-cell network DL and UL PHY-layer security performance under a Poisson field of colluding EDs is depicted in Fig. 2. Similar to the case of passive EDs, increasing the number of antennas always results in higher ergodic secrecy

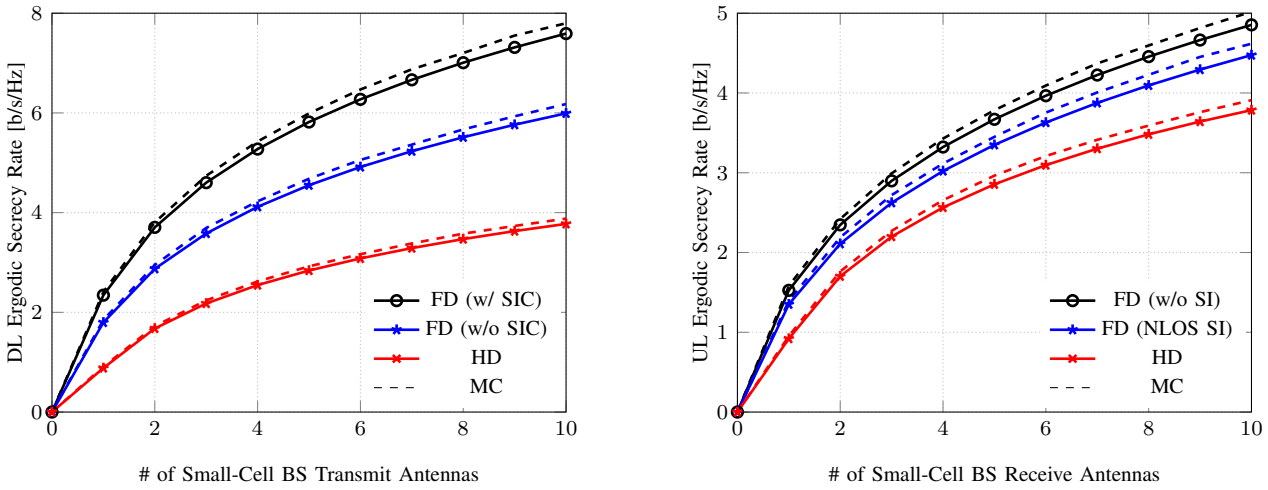

Fig. 2. Impact of the number of BS transmit/receive antennas on the small-cell network PHY-layer security performance under a Poisson field of colluding EDs. System parameters are: $\lambda_d = \frac{4}{\pi}$ km^{-2}, $\lambda_u = K_u\lambda_d$ km^{-2}, $\lambda_e = \frac{\lambda_d}{200}$ km^{-2}, $r_0 = \frac{1}{2}$ km, $K_d = K_u = 1$, $p_d = 23$ dBm, $p_u = 20$ dBm, $W = 10$ MHz, $\sigma_o^2 = \sigma_v^2 = \sigma_i^2 = \sigma_c^2 = -170$ dBm/Hz, $\alpha = 4$.

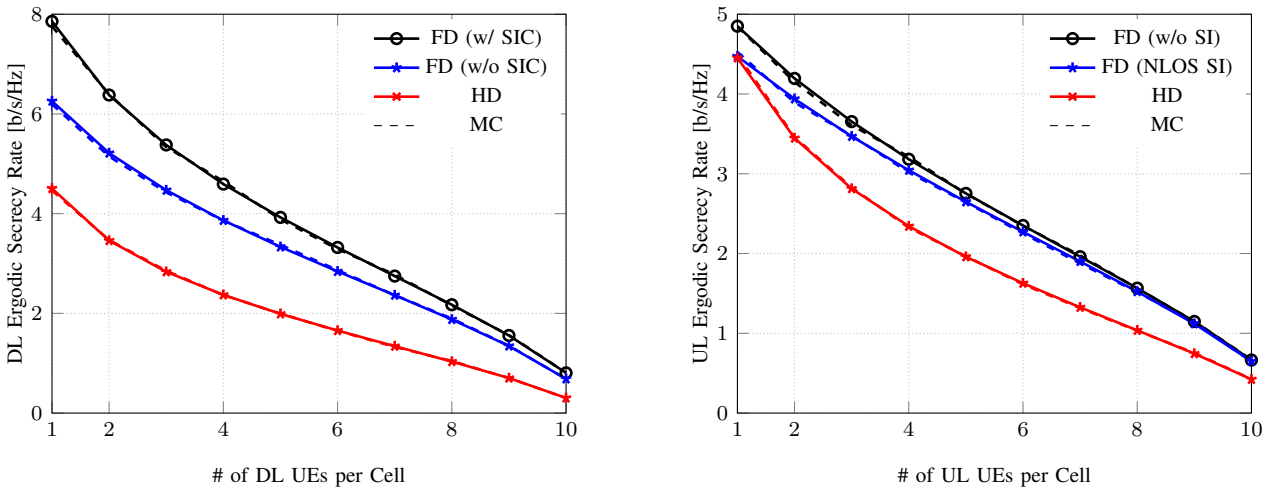

Fig. 3. Impact of the number of UEs on the small-cell network PHY-layer security performance in the presence of a Poisson field of passive EDs. System parameters are: $\lambda_d = \frac{4}{\pi}$ km^{-2}, $\lambda_u = K_u\lambda_d$ km^{-2}, $\lambda_e = \frac{\lambda_d}{5}$ km^{-2}, $N_d = N_u = 10$, $p_d = 23$ dBm, $p_u = 20$ dBm, $W = 10$ MHz, $\sigma_o^2 = \sigma_v^2 = \sigma_i^2 = \sigma_c^2 = -170$ dBm/Hz, $\alpha = 4$.

rates, as well as greater FD versus HD PHY-layer security performance gains. Furthermore, our findings indicate that the relative FD versus HD ergodic secrecy rate gain can be considerably higher in the case of colluding EDs. The reason is because each cooperative ED experiences added interference (i.e., MI) in the case of FD operation which in turn degrades the colluding EDs' combined SINR. It is important to note that the case of collusion represents the absolute worst-case scenario in terms of PHY-layer security performance. As a result, unless the EDs' spatial density is set to very small values (relative to the BS deployment density), the small-cell network experiences secrecy outage with high probability. It should be noted that the MC results from Fig. 2 confirm the validity of our findings in *Theorems 1-2* and *Theorems 5-6*.

B. Impact of the Number of Users

1) Passive Eavesdropping: We investigate the impact of the number of users served per resource block on the small-cell network DL and UL PHY-layer security performances under a Poisson field of passive EDs in Fig. 3. The results indicate that the per-user ergodic secrecy rate performance in all systems always decreases in the number of UEs served per cell. On the other hand, it should be noted that the corresponding ergodic area secrecy rate (e.g., $\lambda_d K_d S_o$ (b/s/Hz/km^2), in the DL) increases with higher number of users served per resource block. The reason is that with greater K_d and K_d, respectively, the DL and UL array gains are decreased due to the linear ZF beamforming. In addition, increasing K_d and K_u results in higher MI in the UL and DL, respectively. As a result, it can be inferred that the FD versus HD small-cell network PHY-layer security performance gain decreases as we increase the number of DL and UL UEs served per cell. Intuitively, if we keep K_u fixed, increasing K_d results in higher FD versus HD DL ergodic area secrecy rate (and vice versa). In addition, it should be noted that the importance of effective interference cancellation is heightened in the case of FD small-cell BSs

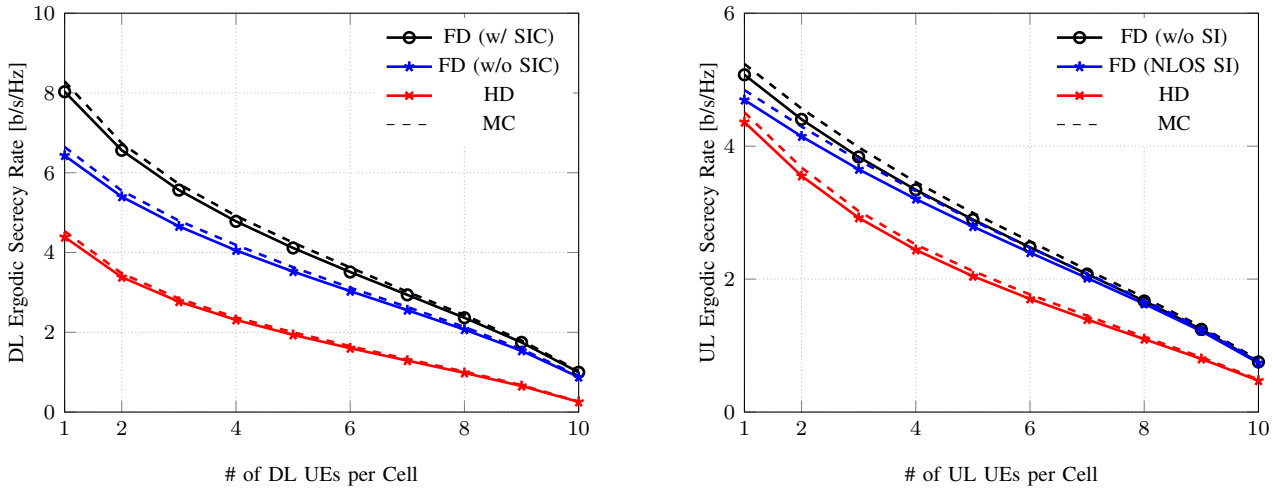

Fig. 4. Impact of the number of UEs on the small-cell network PHY-layer security performance in the presence of a Poisson field of colluding EDs. System parameters are: $\lambda_d = \frac{4}{\pi}$ km^{-2}, $\lambda_u = K_u\lambda_d$ km^{-2}, $\lambda_e = \frac{\lambda_d}{400}$ km^{-2}, $r_0 = \frac{1}{2}$ km, $N_d = N_u = 10$, $p_d = 23$ dBm, $p_u = 20$ dBm, $W = 10$ MHz, $\sigma_o^2 = \sigma_v^2 = \sigma_i^2 = \sigma_c^2 = -170$ dBm/Hz, $\alpha = 4$.

serving more UEs, such to avoid secrecy outage scenarios.

2) Colluding Eavesdropping: In Fig. 4, we study the effect of the number of users served per resource block on the small-cell network DL and UL PHY-layer security performances under a Poisson field of colluding EDs. The trends previously highlighted in the case of passive PPP-based EDs also apply here. In particular, increasing the number of UEs served per cell deceases the per-user ergodic secrecy rate and increases the area ergodic secrecy rate, respectively. Also, in the case of large-scale ED collusion, the FD over HD small-cell network PHY-layer security performance gain decreases if we simultaneously increase the number of DL and UL UEs served per cell. On the other hand, for a given number of UL UEs in a cell, increasing the number of DL UEs served per resource block results in higher relative FD versus HD DL ergodic secrecy rate (and vice versa).

C. Impact of the Eavesdroppers' Density

1) Passive Eavesdroppers: Next, we proceed by investigating the impact of the EDs' spatial density on the small-cell network DL and UL PHY-layer security performances under a PPP-based abstraction model of passive EDs in Fig. 5. As expected, it can be observed that the ergodic secrecy rate decreases in all cases in the ratio of ED over BS deployment densities. Moreover, increasing the spatial density of the EDs enhances the FD versus HD small-cell network PHY-layer security performance gain. This is because while the stronger ED channel capacity degrades the ergodic secrecy rate values, the respective rate of decrease in the PHY-layer security performance is higher in HD versus FD small-cell networks as a result of the extra interference experienced by the EDs in the latter system. As previously highlighted, the relative FD versus HD UL ergodic secrecy gain can be increased through reducing the transmit power of the small-cell BSs.

2) Colluding Eavesdroppers: Finally, the effect of EDs' spatial density on the small-cell network PHY-layer security performance in the presence of a Poisson field of colluding EDs is depicted in Fig. 6. We can observe similar trends to those highlighted in the case of passive EDs. In particular, the PHY-layer security performance benefits in all cases from smaller ED PPP-based deployment density. Moreover, the underlying FD versus HD gains in terms of ergodic secrecy rate increases with larger values of λ_e up to the point in which the system experiences secrecy outage. In addition, as previously highlighted, the UL PHY-layer security performance in the FD small-cell network is particularly susceptible to interference. Hence, enabling multi-antenna communications and interference cancellation capabilities is essential towards avoiding secrecy outage scenarios in the UL.

V. Conclusions

We provided a stochastic geometry-based framework for the study of PHY-layer security performance in multi-cell FD small-cell networks. The locations of the BSs, equipped with multiple antennas, and UEs were captured using the PPP-based abstraction model. The small-cell network was considered to be overlaid with a Poisson field of EDs, with both scenarios of independent as well as cooperative eavesdropping under consideration. By leveraging on the tools from applied probability theory, we derived explicit expressions for the ergodic secrecy rates with closed-form LT functions for the useful and interference signals statistics. Non-linear curve-fitting techniques were further utilized to devise closed-form approximations in certain special cases of interest. With the aid of the proposed analytical model, and MC simulations, we drew network design insights concerning the ergodic secrecy rate performance. In particular, the findings highlighted that significant improvements in PHY-layer security performance can be attained by enabling FD functionality at the BS side, particularly, in conjunction with multi-antenna communications and interference cancellation schemes.

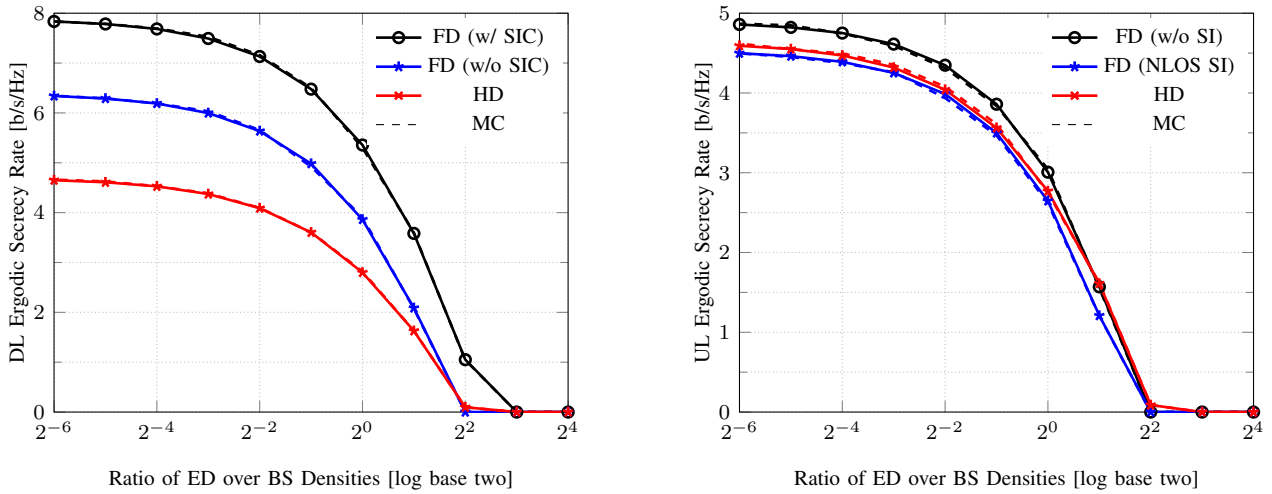

Fig. 5. Impact of different passive EDs' spatial densities on the small-cell network PHY-layer security performance. System parameters are: $\lambda_d = \frac{4}{\pi}$ km^{-2}, $\lambda_u = K_u\lambda_d$ km^{-2}, $N_d = N_u = 8$, $K_d = K_u = 1$, $p_d = 23$ dBm, $p_u = 20$ dBm, $W = 10$ MHz, $\sigma_o^2 = \sigma_v^2 = \sigma_i^2 = \sigma_c^2 = -170$ dBm/Hz, $\alpha = 4$.

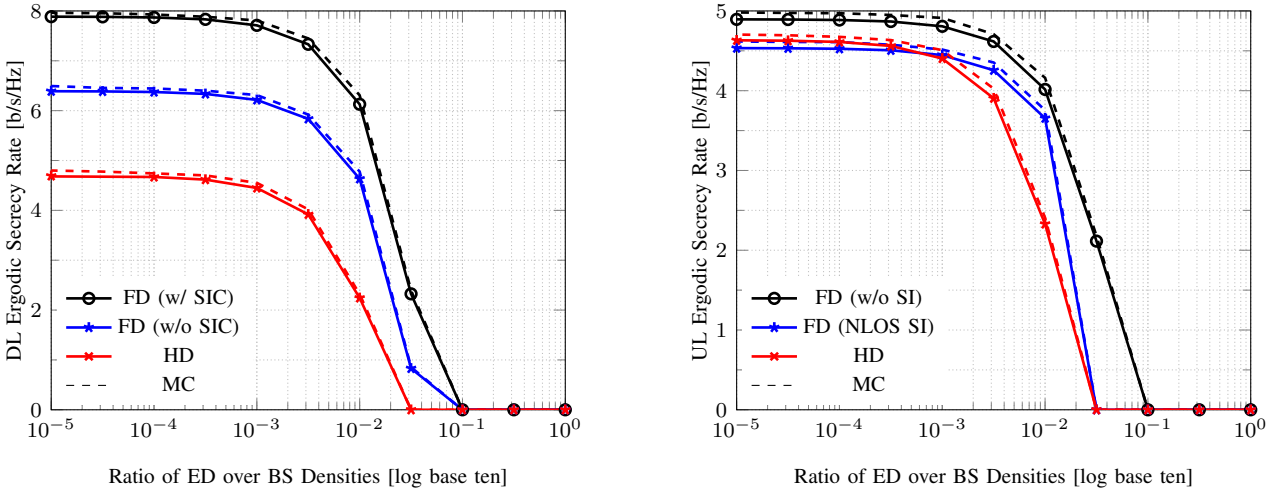

Fig. 6. Impact of different colluding EDs' spatial densities on the small-cell network PHY-layer security performance. System parameters are: $\lambda_d = \frac{4}{\pi}$ km^{-2}, $\lambda_u = K_u\lambda_d$ km^{-2}, $r_0 = \frac{1}{2}$ km, $N_d = N_u = 8$, $K_d = K_u = 1$, $p_d = 23$ dBm, $p_u = 20$ dBm, $W = 10$ MHz, $\sigma_o^2 = \sigma_v^2 = \sigma_i^2 = \sigma_c^2 = -170$ dBm/Hz, $\alpha = 4$.

Appendix A

The ergodic rate (considering FD BSs) for the user o in the DL per resource block can be calculated using

$$C_o^{\text{FD}} = \mathbb{E}\left[\log_2\left(1+\gamma_o^{\text{FD}}\right)\right] = \frac{1}{\ln(2)}\int_0^\infty\int_0^\infty \frac{1-F^{\text{FD}}_{\gamma_o|r_{b,o}=r}[\gamma]}{1+\gamma}\,\mathrm{d}\gamma\,\mathcal{P}_{r_{b,o}}[r]\,\mathrm{d}r \tag{A.1}$$

where

$$F_{\gamma_o^{\text{FD}}|r_{b,o}=r}[\gamma] = \Pr\left[\gamma_o^{\text{FD}} < \gamma \mid r_{b,o} = r\right] = 1 - \Pr\left[G_{b,o} > \frac{\gamma r^\alpha}{p_d}\left(I_o^{d,d} + I_o^{u,d} + \sigma_o^2\right)\right] \overset{(i)}{=} 1 - \sum_{n=0}^{N_d-K_d}\left\{\frac{(-s)^n}{n!}\frac{\mathrm{d}^n}{\mathrm{d}s^n}\exp\left(-s\sigma_o^2\right)\mathscr{L}_{I_o^{d,d}}[s]\mathscr{L}_{I_o^{u,d}}[s]\right\}_{s=\frac{\gamma r^\alpha}{p_d}} \tag{A.2}$$

with (i) written using the identity $x^n f(x) \equiv (-1)^n \frac{\mathrm{d}^n}{\mathrm{d}s^n}\mathcal{L}_{f(x)}[s]$ (a property of LT function). Hence, we arrive at (9).

The LT function of the inter-cell interference at the reference UE in the DL o is given by

$$\mathscr{L}_{I_o^{d,d}}(s) = \mathbb{E}_{\phi_d,G_{l,o}}\left[\exp\left(-s\sum_{l\in\phi_d\setminus\{b\}} p_d G_{l,o} r_{l,o}^{-\alpha}\right)\right] \overset{(i)}{=} \mathbb{E}_{\phi_d}\left[\prod_{l\in\phi_d\setminus\{b\}}\mathbb{E}_{G_{l,o}}\left[\exp\left(-sp_d G_{l,o} r_{l,o}^{-\alpha}\right)\right]\right] \overset{(ii)}{=} \exp\left(-2\pi\lambda_d\int_r^\infty\left(1-\frac{1}{\left(1+sp_d x^{-\alpha}\right)^{K_d}}\right)x\,\mathrm{d}x\right) \overset{(iii)}{=} \exp\left(-\pi\lambda_d r^2\left({}_2F_1\left(K_d,-\frac{2}{\alpha};1-\frac{2}{\alpha};-\frac{sp_d}{r^\alpha}\right)-1\right)\right) \tag{A.3}$$

where (i) follows independence property of PPP and uncorrelated channel conditions [58], (ii) is obtained by applying the probability generating functional (PGFL) of a PPP and converting from Cartesian to polar coordinates [59], and (iii) is written by applying the integral identity $\int_r^{+\infty}\left(1-\left(1+\beta x^{-\alpha}\right)^{-K}\right)x\ \mathrm{d}x = \frac{r^2}{2}\left({}_2F_1\left(-\frac{2}{\alpha},K;1-\frac{2}{\alpha};-\frac{\beta}{r^\alpha}\right)-1\right)$.

Using a similar approach to that in the above, the LT function of the MI at the reference UE in the DL o is given by

$$\begin{aligned}\mathscr{L}_{I_o^{u,d}}(s) &= \mathbb{E}_{\phi_u,G_{k,o}}\left[\exp\left(-s\sum_{k\in\phi_u}p_uG_{k,o}r_{k,o}^{-\alpha}\right)\right]\\ &= \exp\left(-2\pi K_u\lambda_d\int_\varepsilon^\infty\left(1-\frac{1}{1+sp_ux^{-\alpha}}\right)x\ \mathrm{d}x\right)\\ &= \exp\left(-\pi K_u\lambda_d\varepsilon^2\left({}_2F_1\left(1,-\frac{2}{\alpha};1-\frac{2}{\alpha};-\frac{sp_u}{\varepsilon^\alpha}\right)-1\right)\right)\end{aligned} \tag{A.4}$$

where ϵ can be tuned by design or measurements to capture the SIC capability of the UEs. Hence, we arrive at *Theorem 1*. ■

Appendix B

Utilizing a similar approach to that in Appendix A, we can arrive at (13). Moreover, using a similar methodology, the LT functions of the different UL interfering terms for the postcoding of the useful signal at the reference BS are given by

$$\begin{aligned}\mathscr{L}_{I_i^{u,u}}(s) &= \mathbb{E}_{\phi_u,H_{k,i}}\left[\exp\left(-s\sum_{k\in\hat{\phi}_u}p_uH_{k,i}r_{k,i}^{-\alpha}\right)\right]\\ &= \exp\left(-2\pi K_u\lambda_d\int_r^\infty\left(1-\frac{1}{1+sp_ux^{-\alpha}}\right)x\ \mathrm{d}x\right)\\ &= \exp\left(-\pi K_u\lambda_dr^2\left({}_2F_1\left(1,-\frac{2}{\alpha};1-\frac{2}{\alpha};-\frac{sp_u}{r^\alpha}\right)-1\right)\right)\end{aligned} \tag{B.1}$$

$$\begin{aligned}\mathscr{L}_{I_i^{d,u}}(s) &= \mathbb{E}_{\phi_d,H_{l,i}}\left[\exp\left(-s\sum_{l\in\phi_d}p_dH_{l,i}r_{l,i}^{-\alpha}\right)\right]\\ &= \exp\left(-2\pi\lambda_d\int_0^\infty\left(1-\frac{1}{\left(1+sp_dx^{-\alpha}\right)^{K_d}}\right)x\ \mathrm{d}x\right)\\ &= \exp\left(-\pi\lambda_d\left(sp_d\right)^{\frac{2}{\alpha}}\frac{\Gamma\left(1-\frac{2}{\alpha}\right)\Gamma\left(K_d+\frac{2}{\alpha}\right)}{\Gamma(K_d)}\right)\end{aligned} \tag{B.2}$$

and

$$\mathscr{L}_{I_i^{b,b}}(s) = \left(1+sp_d\theta\right)^{-\kappa}. \tag{B.3}$$

Hence, we arrive at *Theorem 2*. ■

Appendix C

The ergodic rate (considering FD BSs) of the most malicious passive ED in the DL v per resource block can be calculated using

$$C_v^{\mathrm{FD}} = \mathbb{E}\left[\log_2\left(1+\gamma_v^{\mathrm{FD}}\right)\right] = \frac{1}{\ln(2)}\int_0^\infty\frac{1-F_{\gamma_v}^{\mathrm{FD}}[\gamma]}{1+\gamma}\ \mathrm{d}\gamma \tag{C.1}$$

where

$$\begin{aligned}F_{\gamma_v^{\mathrm{FD}}}[\gamma] &= \Pr[\gamma_v^{\mathrm{FD}}<\gamma] = \Pr\left[\max_{e\in\phi_e}\left(\frac{p_dG_{b,e}r_{b,e}^{-\alpha}}{I_e^{d,d}+I_e^{u,d}+\sigma_e^2}\right)<\gamma\right]\\ &= \mathbb{E}_{\phi_e}\left[\prod_{e\in\phi_e}\Pr\left(\frac{p_dG_{b,e}r_{b,e}^{-\alpha}}{I_e^{d,d}+I_e^{u,d}+\sigma_e^2}<\gamma\mid\phi_e\right)\right]\overset{(i)}{=}\\ &\exp\left(-2\pi\lambda_e\int_0^\infty\left(1-\Pr\left[\frac{p_dG_{b,v}r^{-\alpha}}{I_v^{d,d}+I_v^{u,d}+\sigma_v^2}<\gamma\right]\right)r\ \mathrm{d}r\right)\end{aligned} \tag{C.2}$$

with (i) obtained using the PGFL of a PPP and converting from Cartesian to polar coordinates. The probability from the above is given by

$$\begin{aligned}&1-\Pr\left[\frac{p_dG_{b,v}r^{-\alpha}}{I_v^{d,d}+I_v^{u,d}+\sigma_v^2}<\gamma\right]\\ &= \Pr\left[G_{b,v}>\frac{\gamma r^\alpha}{p_d}\left(I_v^{d,d}+I_v^{u,d}+\sigma_v^2\right)\right]\\ &= \left\{\exp\left(-s\sigma_v^2\right)\mathscr{L}_{I_v^{d,d}}(s)\mathscr{L}_{I_v^{u,d}}(s)\right\}_{s=\frac{\gamma r^\alpha}{p_d}}.\end{aligned} \tag{C.3}$$

Hence, we arrive at (18).

The LT function of the inter-cell interference at the most malicious ED in the DL v is given by

$$\begin{aligned}\mathscr{L}_{I_v^{d,d}}(s) &= \mathbb{E}_{\phi_d,G_{l,v}}\left[\exp\left(-s\sum_{l\in\phi_d}p_dG_{l,v}r_{l,v}^{-\alpha}\right)\right]\\ &\overset{(i)}{=} \mathbb{E}_{\phi_d}\left[\prod_{l\in\phi_d}\mathbb{E}_{G_{l,v}}\left[\exp\left(-sp_dG_{l,v}r_{l,v}^{-\alpha}\right)\right]\right]\\ &\overset{(ii)}{=} \exp\left(-2\pi\lambda_d\int_0^\infty\left(1-\frac{1}{\left(1+sp_dx^{-\alpha}\right)^{K_d}}\right)x\ \mathrm{d}x\right)\\ &\overset{(iii)}{=} \exp\left(-\pi\lambda_d\left(sp_d\right)^{\frac{2}{\alpha}}\frac{\Gamma\left(1-\frac{2}{\alpha}\right)\Gamma\left(K_d+\frac{2}{\alpha}\right)}{\Gamma(K_d)}\right)\end{aligned} \tag{C.4}$$

where (i) follows from the independence property of PPP and uncorrelated channel conditions, (ii) is obtained using the PGFL of a PPP and converting from Cartesian to polar coordinates, and (iii) is written using the integral identity $\int_0^{+\infty}\left(1-\left(1+\beta x^{-\alpha}\right)^{-K}\right)x\ \mathrm{d}x = \frac{\beta^{\frac{2}{\alpha}}\Gamma\left(1-\frac{2}{\alpha}\right)\Gamma\left(K+\frac{2}{\alpha}\right)}{2\Gamma(K)}$.

Using a similar approach to that in the above, the LT function of the MI at the most malicious ED in the DL v is given by

$$\begin{aligned}\mathscr{L}_{I_v^{u,d}}(s) &= \mathbb{E}_{\phi_u,G_{k,v}}\left[\exp\left(-s\sum_{k\in\phi_u}p_uG_{k,v}r_{k,v}^{-\alpha}\right)\right]\\ &= \exp\left(-2\pi K_u\lambda_d\int_0^\infty\left(1-\frac{1}{1+sp_ux^{-\alpha}}\right)x\ \mathrm{d}x\right)\end{aligned}$$

$$= \exp\left(-\pi K_u \lambda_d \left(s p_u\right)^{\frac{2}{\alpha}} \Gamma\left(1-\frac{2}{\alpha}\right) \Gamma\left(1+\frac{2}{\alpha}\right)\right). \quad \text{(C.5)}$$

Hence, we arrive at *Theorem 3*. ■

APPENDIX D

Utilizing a similar approach to that in Appendix C, we can arrive at (22). Moreover, using a similar methodology, the LT functions of the different UL interfering terms at the most malicious ED c are given by

$$\mathscr{L}_{I_c^{u,u}}(s) = \mathbb{E}_{\phi_u, H_{k,c}}\left[\exp\left(-s \sum_{k \in \phi_u} p_u H_{k,c} r_{k,c}^{-\alpha}\right)\right]$$
$$= \exp\left(-2\pi K_u \lambda_d \int_0^\infty \left(1 - \frac{1}{1+s p_u x^{-\alpha}}\right) x \, \mathrm{d}x\right)$$
$$= \exp\left(-\pi K_u \lambda_d \left(s p_u\right)^{\frac{2}{\alpha}} \Gamma\left(1-\frac{2}{\alpha}\right) \Gamma\left(1+\frac{2}{\alpha}\right)\right) \quad \text{(D.1)}$$

and

$$\mathscr{L}_{I_c^{d,u}}(s) = \mathbb{E}_{\phi_d, H_{l,c}}\left[\exp\left(-s \sum_{l \in \phi_d} p_d H_{l,c} r_{l,c}^{-\alpha}\right)\right]$$
$$= \exp\left(-2\pi \lambda_d \int_0^\infty \left(1 - \frac{1}{\left(1+s p_d x^{-\alpha}\right)^{K_d}}\right) x \, \mathrm{d}x\right)$$
$$= \exp\left(-\pi \lambda_d \left(s p_d\right)^{\frac{2}{\alpha}} \frac{\Gamma\left(1-\frac{2}{\alpha}\right) \Gamma\left(K_d+\frac{2}{\alpha}\right)}{\Gamma(K_d)}\right). \quad \text{(D.2)}$$

Hence, we arrive at *Theorem 4*. ■

APPENDIX E

The ergodic rate (considering FD BSs) of the most malicious colluding ED in the DL v per resource block can be calculated using

$$C_v^{\mathrm{FD}} = \mathbb{E}\left[\log_2\left(1+\gamma_v^{\mathrm{FD}}\right)\right] = \frac{1}{\ln(2)} \int_0^\infty \frac{1 - F_{\gamma_v}^{\mathrm{FD}}[\gamma]}{1+\gamma} \, \mathrm{d}\gamma \quad \text{(E.1)}$$

where

$$1 - F_{\gamma_v^{\mathrm{FD}}}[\gamma] = \Pr[\gamma_v^{\mathrm{FD}} > \gamma]$$
$$= \Pr\left[\sum_{e \in \phi_e} \left(\frac{p_d G_{b,e} r_{b,e}^{-\alpha}}{I_e^{d,d} + I_e^{u,d} + \sigma_e^2}\right) > \gamma\right]$$
$$\overset{(i)}{\leq} \frac{1}{\gamma} \mathbb{E}\left[\sum_{e \in \phi_e} \left(\frac{p_d G_{b,e} r_{b,e}^{-\alpha}}{I_e^{d,d} + I_e^{u,d} + \sigma_e^2}\right)\right]$$
$$\overset{(ii)}{=} \frac{2\pi\lambda_e}{\gamma} \int_{r_0}^\infty \mathbb{E}\left[\frac{p_d G_{b,e} r^{-\alpha}}{I_e^{d,d} + I_e^{u,d} + \sigma_e^2}\right] r \, \mathrm{d}r$$
$$\overset{(iii)}{=} \frac{2\pi\lambda_e}{\gamma} \int_{r_0}^\infty \mathbb{E}\left[p_d G_{b,v} r^{-\alpha}\right] \int_0^\infty \exp\left(-s\sigma_v^2\right)$$
$$\times \mathscr{L}_{I_e^{d,d}}[s] \mathscr{L}_{I_v^{u,d}}[s] \, \mathrm{d}s \, r \, \mathrm{d}r$$
$$\overset{(iv)}{=} \frac{2\pi\lambda_e p_d}{\gamma} \int_{r_0}^\infty r^{1-\alpha} \int_0^\infty \exp\left(-s\sigma_v^2\right)$$
$$\times \mathscr{L}_{I_e^{d,d}}[s] \mathscr{L}_{I_v^{u,d}}[s] \, \mathrm{d}s \, \mathrm{d}r \quad \text{(E.2)}$$

with (i) is written using the Markov inequality, (ii) follows from applying the Campbell's theorem to a sum over PPP and converting from Cartesian to polar coordinates [59], (iii) is obtained using the approach from [60] for calculating the moments of SINR, and (iv) is given by taking the average over the ED useful signal. Hence, we arrive at *Theorem 5*. ■

APPENDIX F

Here, we provide some numerical examples in order to demonstrate the validity of the approximate expressions developed in *Corollaries 1-8* for some special cases of interest.

In Fig. F.1, we present the ergodic rate performance of the intended DL and UL UEs versus different number of small-cell BS antennas for the special case described in *Corollaries 1-2*.

Next, we depict the ergodic rate performance of the most malicious DL and UL EDs versus different EDs' spatial densities in Fig. F.2. The results are obtained considering passive EDs as in *Corollary 3*, and colluding EDs as in *Corollary 4*, respectively.

The DL and UL ergodic secrecy rates in the FD and HD small-cell networks in the presence of a Poisson field of passive EDs under the system parameters described in *Corollaries 5-6* are depicted in Fig. F.3. Finally, the corresponding PHY-layer security performance in the presence of PPP-based colluding EDs for the special case described in *Corollaries 7-8* is shown in Fig. F.4.

The numerical examples provided in this Appendix confirm the validity of the approximate expressions in *Corollaries 1-8*. ■

REFERENCES

[1] A. Babaei, A. H. Aghvami, A. Shojaeifard, and K. K. Wong, "Physical layer security in full-duplex cellular networks," in *IEEE Int. Symp. Personal Indoor Mobile Radio Commun. (PIMRC)*, Oct. 2017.

[2] ——, "Full-duplex MIMO small-cells: Secrecy capacity analysis," in *IEEE Veh. Technol. Conf. (VTC-Spring)*, June 2018.

[3] M. Duarte, C. Dick, and A. Sabharwal, "Experiment-driven characterization of full-duplex wireless systems," *IEEE Trans. Wireless Commun.*, vol. 11, no. 12, pp. 4296–4307, Dec. 2012.

[4] A. Sabharwal, P. Schniter, D. Guo, D. W. Bliss, S. Rangarajan, and R. Wichman, "In-band full-duplex wireless: Challenges and opportunities," *IEEE J. Sel. Areas Commun.*, vol. 32, no. 9, pp. 1637–1652, Sept. 2014.

[5] A. Khandani, "Methods for spatial multiplexing of wireless two-way channels," Oct. 2010, US Patent 7,817,641.

[6] J. I. Choi, M. Jain, K. Srinivasan, P. Levis, and S. Katti, "Achieving single channel, full duplex wireless communication," in *Proc. MobiCom*. ACM, 2010.

[7] T. Riihonen, S. Werner, and R. Wichman, "Mitigation of loopback self-interference in full-duplex MIMO relays," *IEEE Trans. Signal Process.*, vol. 59, no. 12, pp. 5983–5993, Dec. 2011.

[8] E. Everett, A. Sahai, and A. Sabharwal, "Passive self-interference suppression for full-duplex infrastructure nodes," *IEEE Trans. Wireless Commun.*, vol. 13, no. 2, pp. 680–694, Feb. 2014.

[9] D. Kim, H. Lee, and D. Hong, "A survey of in-band full-duplex transmission: From the perspective of PHY and MAC layers," *IEEE Commun. Surveys Tuts.*, vol. 17, no. 4, pp. 2017–2046, Fourth Quart. 2015.

[10] A. Sezgin, A. S. Avestimehr, M. A. Khajehnejad, and B. Hassibi, "Divide-and-conquer: Approaching the capacity of the two-pair bidirectional Gaussian relay network," *IEEE Trans. Inf. Theory*, vol. 58, no. 4, pp. 2434–2454, Apr. 2012.

[11] C. Wang, H. Farhadi, and M. Skoglund, "Achieving the degrees of freedom of wireless multi-user relay networks," *IEEE Trans. Commun.*, vol. 60, no. 9, pp. 2612–2622, Sept. 2012.

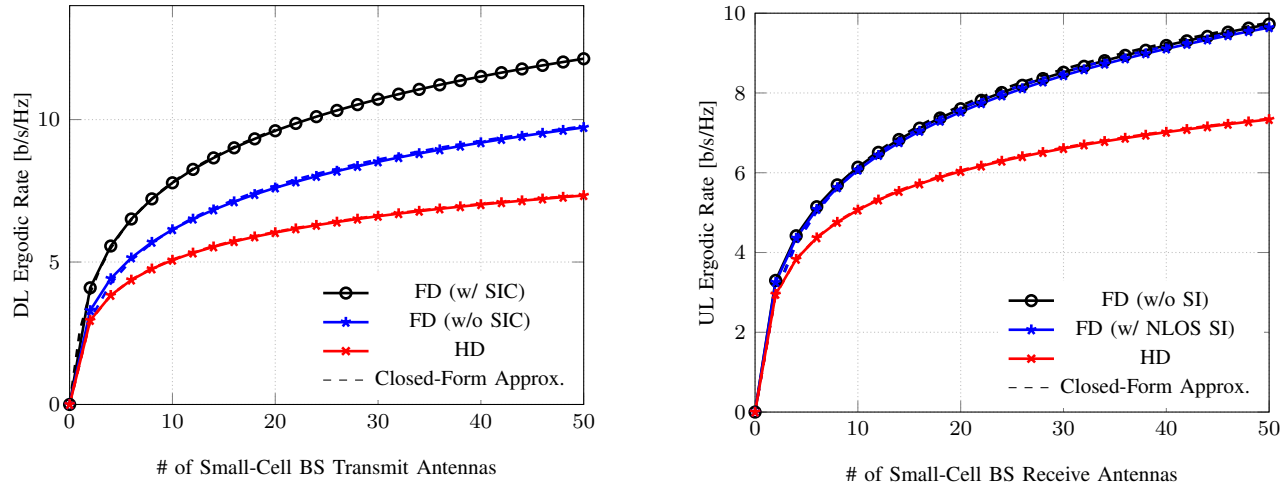

Fig. F.1. Ergodic rates of the intended DL and UL UEs versus the number of small-cell BS antennas. System parameters are: $K_d = K_u = 1$, $\sigma_o^2 = \sigma_i^2 = 0$, $\alpha = 4$.

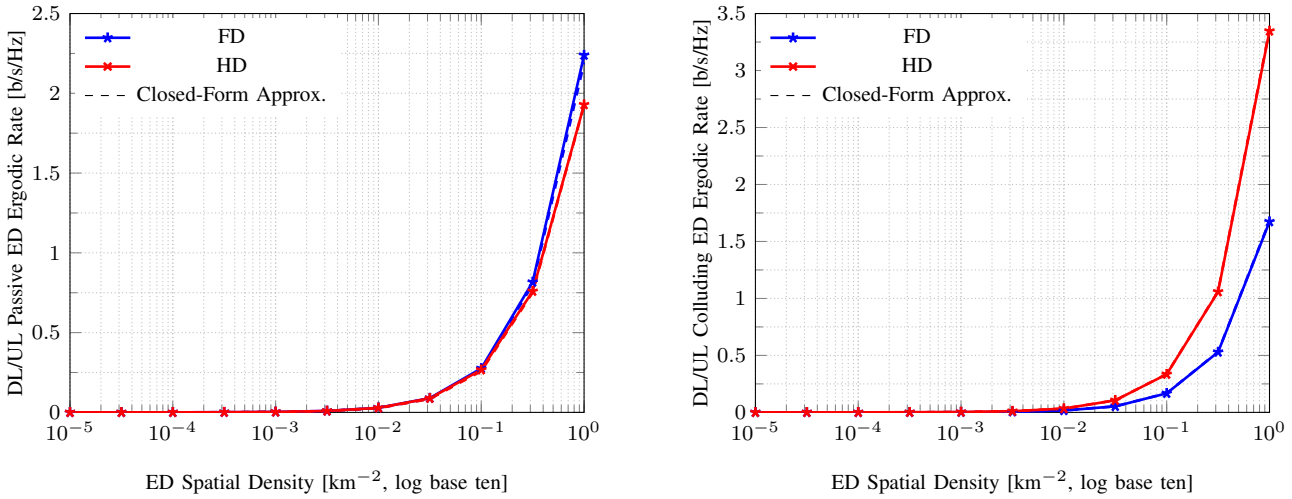

Fig. F.2. Ergodic rates of the most malicious DL and UL EDs versus the EDs' spatial densities. System parameters are: $r_0 = 5$ m (in case of collusion), $K_d = K_u = 1$, $\sigma_v^2 = \sigma_c^2 = 0$, $\alpha = 4$.

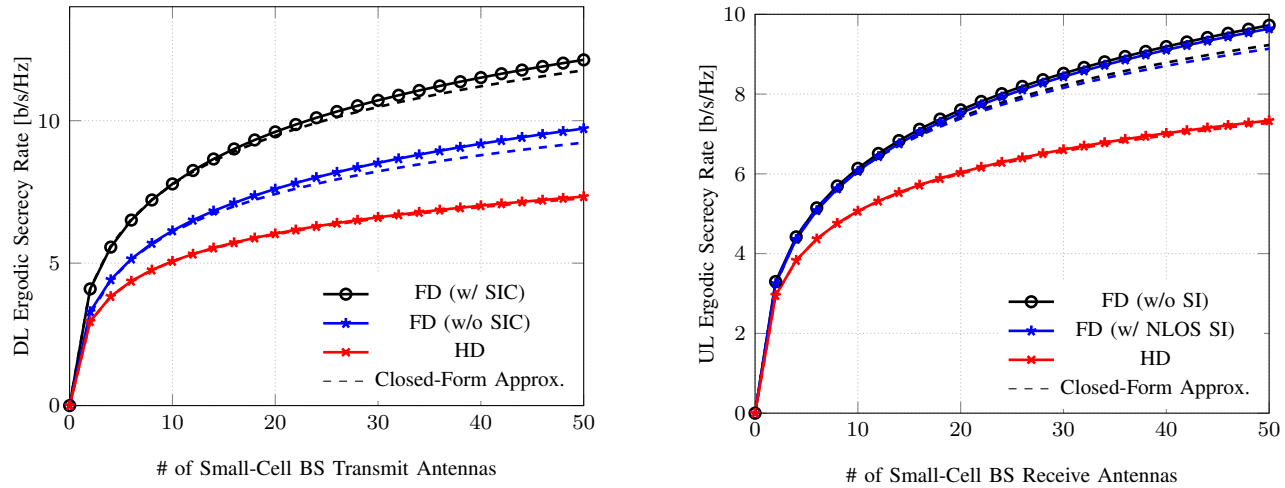

Fig. F.3. Ergodic secrecy rate in the presence of a Poisson field of passive EDs versus the number of small-cell BS antennas. System parameters are: $\lambda_e = 10^{-6}$ km^{-2}, $K_d = K_u = 1$, $\sigma_o^2 = \sigma_v^2 = \sigma_i^2 = \sigma_c^2 = 0$.

[12] D. Nguyen, L. N. Tran, P. Pirinen, and M. Latva-aho, "On the spectral efficiency of full-duplex small cell wireless systems," *IEEE Trans.*

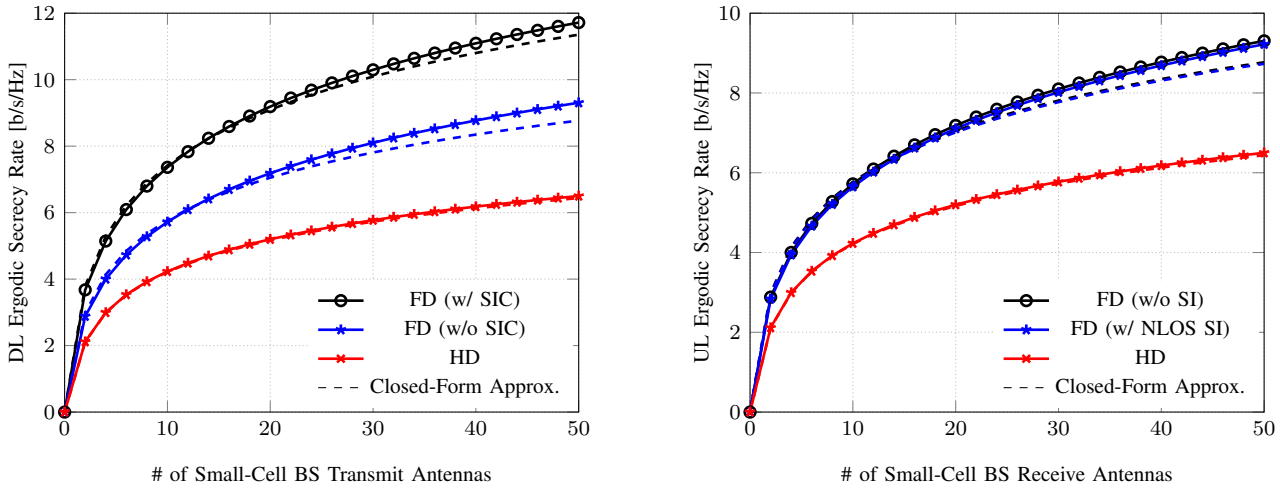

Fig. F.4. Ergodic secrecy rate in the presence of a Poisson field of colluding EDs versus the number of small-cell BS antennas. System parameters are: $\lambda_e = 10^{-4}$ km^{-2}, $r_0 = 0.1$ m, $K_d = K_u = 1$, $\sigma_o^2 = \sigma_v^2 = \sigma_i^2 = \sigma_c^2 = 0$.

Wireless Commun., vol. 13, no. 9, pp. 4896–4910, Sept. 2014.

[13] Z. Tong and M. Haenggi, "Throughput analysis for full-duplex wireless networks with imperfect self-interference cancellation," *IEEE Trans. Commun.*, vol. 63, no. 11, pp. 4490–4500, Nov. 2015.

[14] H. Tabassum, A. H. Sakr, and E. Hossain, "Analysis of massive MIMO-enabled downlink wireless backhauling for full-duplex small cells," *IEEE Trans. Commun.*, vol. 64, no. 6, pp. 2354–2369, June 2016.

[15] I. Atzeni and M. Kountouris, "Full-duplex MIMO small-cell networks with interference cancellation," *IEEE Trans. Wireless Commun.*, vol. 16, no. 12, pp. 8362–8376, Dec. 2017.

[16] A. Gupta and R. K. Jha, "A survey of 5G network: Architecture and emerging technologies," *IEEE Access*, vol. 3, pp. 1206–1232, July 2015.

[17] A. Mukherjee, S. A. A. Fakoorian, J. Huang, and A. L. Swindlehurst, "Principles of physical layer security in multiuser wireless networks: A survey," *IEEE Commun. Surveys Tuts.*, vol. 16, no. 3, pp. 1550–1573, Third Quart. 2014.

[18] A. D. Wyner, "The wire-tap channel," *Bell Labs Technical Journal*, vol. 54, no. 8, pp. 1355–1387, 1975.

[19] L. Dong, Z. Han, A. P. Petropulu, and H. V. Poor, "Improving wireless physical layer security via cooperating relays," *IEEE Trans. Signal Process.*, vol. 58, no. 3, pp. 1875–1888, Mar. 2010.

[20] G. Zheng, L. C. Choo, and K. K. Wong, "Optimal cooperative jamming to enhance physical layer security using relays," *IEEE Trans. Signal Process.*, vol. 59, no. 3, pp. 1317–1322, Mar. 2011.

[21] J. Li, A. P. Petropulu, and S. Weber, "On cooperative relaying schemes for wireless physical layer security," *IEEE Trans. Signal Process.*, vol. 59, no. 10, pp. 4985–4997, Oct. 2011.

[22] Y. Zou, X. Wang, and W. Shen, "Physical-layer security with multiuser scheduling in cognitive radio networks," *IEEE Trans. Commun.*, vol. 61, no. 12, pp. 5103–5113, Dec. 2013.

[23] M. Elkashlan, L. Wang, T. Q. Duong, G. K. Karagiannidis, and A. Nallanathan, "On the security of cognitive radio networks," *IEEE Trans. Veh. Technol.*, vol. 64, no. 8, pp. 3790–3795, Aug. 2015.

[24] T. Lv, H. Gao, and S. Yang, "Secrecy transmit beamforming for heterogeneous networks," *IEEE J. Sel. Areas Commun.*, vol. 33, no. 6, pp. 1154–1170, June 2015.

[25] D. W. K. Ng, E. S. Lo, and R. Schober, "Robust beamforming for secure communication in systems with wireless information and power transfer," *IEEE Trans. Wireless Commun.*, vol. 13, no. 8, pp. 4599–4615, Aug. 2014.

[26] L. Wang, K. K. Wong, M. Elkashlan, A. Nallanathan, and S. Lambotharan, "Secrecy and energy efficiency in massive MIMO aided heterogeneous C-RAN: A new look at interference," *IEEE J. Sel. Topics Signal Process.*, vol. 10, no. 8, pp. 1375–1389, Dec. 2016.

[27] X. Zhou, R. K. Ganti, J. G. Andrews, and A. Hjørungnes, "On the throughput cost of physical layer security in decentralized wireless networks," *IEEE Trans. Wireless Commun.*, vol. 10, no. 8, pp. 2764–2775, Aug. 2011.

[28] T. X. Zheng, H. M. Wang, and Q. Yin, "On transmission secrecy outage of a multi-antenna system with randomly located eavesdroppers," *IEEE Commun. Lett.*, vol. 18, no. 8, pp. 1299–1302, Aug. 2014.

[29] T. X. Zheng, H. M. Wang, J. Yuan, D. Towsley, and M. H. Lee, "Multi-antenna transmission with artificial noise against randomly distributed eavesdroppers," *IEEE Trans. Commun.*, vol. 63, no. 11, pp. 4347–4362, Nov. 2015.

[30] G. Chen and J. P. Coon, "Secrecy outage analysis in random wireless networks with antenna selection and user ordering," *IEEE Wireless Commun. Lett.*, vol. 6, no. 3, pp. 334–337, June 2017.

[31] G. Chen, J. P. Coon, and M. D. Renzo, "Secrecy outage analysis for downlink transmissions in the presence of randomly located eavesdroppers," *IEEE Trans. Inf. Forensics Security*, vol. 12, no. 5, pp. 1195–1206, May 2017.

[32] G. Liu, F. R. Yu, H. Ji, V. C. M. Leung, and X. Li, "In-band full-duplex relaying: A survey, research issues and challenges," *IEEE Commun. Surveys Tuts.*, vol. 17, no. 2, pp. 500–524, Second Quart. 2015.

[33] G. Zheng, I. Krikidis, J. Li, A. P. Petropulu, and B. Ottersten, "Improving physical layer secrecy using full-duplex jamming receivers," *IEEE Trans. Signal Process.*, vol. 61, no. 20, pp. 4962–4974, Oct. 2013.

[34] G. Chen, Y. Gong, P. Xiao, and J. A. Chambers, "Physical layer network security in the full-duplex relay system," *IEEE Trans. Inf. Forensics Security*, vol. 10, no. 3, pp. 574–583, Mar. 2015.

[35] ——, "Dual antenna selection in secure cognitive radio networks," *IEEE Trans. Veh. Technol.*, vol. 65, no. 10, pp. 7993–8002, Oct. 2016.

[36] A. E. Shafie, A. Sultan, and N. Al-Dhahir, "Physical-layer security of a buffer-aided full-duplex relaying system," *IEEE Commun. Lett.*, vol. 20, no. 9, pp. 1856–1859, Sept. 2016.

[37] T. X. Zheng, H. M. Wang, Q. Yang, and M. H. Lee, "Safeguarding decentralized wireless networks using full-duplex jamming receivers," *IEEE Trans. Wireless Commun.*, vol. 16, no. 1, pp. 278–292, Jan. 2017.

[38] T. X. Zheng, H. M. Wang, J. Yuan, Z. Han, and M. H. Lee, "Physical layer security in wireless ad hoc networks under a hybrid full-/half-duplex receiver deployment strategy," *IEEE Trans. Wireless Commun.*, vol. 16, no. 6, pp. 3827–3839, June 2017.

[39] R. Li, Y. Chen, G. Y. Li, and G. Liu, "Full-duplex cellular networks," *IEEE Commun. Mag.*, vol. 55, no. 4, pp. 184–191, Apr. 2017.

[40] A. Shojaeifard, K. K. Wong, M. D. Renzo, G. Zheng, K. A. Hamdi, and J. Tang, "Massive MIMO-enabled full-duplex cellular networks," *IEEE Trans. Commun.*, vol. 65, no. 11, pp. 4734–4750, Nov. 2017.

[41] D. Stoyan, *Stochastic Geometry and Its Applications*. Chichester New York: Wiley, 1995.

[42] Q. Ye, B. Rong, Y. Chen, M. Al-Shalash, C. Caramanis, and J. G. Andrews, "User association for load balancing in heterogeneous cellular networks," *IEEE Trans. Wireless Commun.*, vol. 12, no. 6, pp. 2706–2716, June 2013.

[43] A. H. Sakr and E. Hossain, "On user association in multi-tier full-duplex cellular networks," *IEEE Trans. Commun.*, vol. 65, no. 9, pp. 4080–4095, Sept. 2017.

[44] H. ElSawy and E. Hossain, "On stochastic geometry modeling of cellular uplink transmission with truncated channel inversion power control," *IEEE Trans. Wireless Commun.*, vol. 13, no. 8, pp. 4454–4469, Aug. 2014.

[45] T. D. Novlan, H. S. Dhillon, and J. G. Andrews, "Analytical modeling of uplink cellular networks," *IEEE Trans. Wireless Commun.*, vol. 12, no. 6, pp. 2669–2679, June 2013.

[46] M. D. Renzo and P. Guan, "Stochastic geometry modeling and system-level analysis of uplink heterogeneous cellular networks with multi-antenna base stations," *IEEE Trans. Commun.*, vol. 64, no. 6, pp. 2453–2476, June 2016.

[47] S. Vuppala and G. Abreu, "Asymptotic secrecy analysis of random networks with colluding eavesdroppers," *IEEE Syst. J.*, accepted 2016.

[48] S. Jia, J. Zhang, H. Zhao, and R. Zhang, "Relay selection for improved security in cognitive relay networks with jamming," *IEEE Wireless Commun. Lett.*, vol. 6, no. 5, pp. 662–665, Oct. 2017.

[49] A. Shojaeifard, K. K. Wong, M. D. Renzo, G. Zheng, K. A. Hamdi, and J. Tang, "Self-interference in full-duplex multi-user MIMO channels," *IEEE Commun. Lett.*, vol. 21, no. 4, pp. 841–844, Apr. 2017.

[50] A. M. Hunter, J. G. Andrews, and S. Weber, "Transmission capacity of ad hoc networks with spatial diversity," *IEEE Trans. Wireless Commun.*, vol. 7, no. 12, pp. 5058–5071, Dec. 2008.

[51] V. Chandrasekhar, M. Kountouris, and J. G. Andrews, "Coverage in multi-antenna two-tier networks," *IEEE Trans. Wireless Commun.*, vol. 8, no. 10, pp. 5314–5327, Oct. 2009.

[52] A. Shojaeifard, K. A. Hamdi, E. Alsusa, D. K. C. So, J. Tang, and K. K. Wong, "Design, modeling, and performance analysis of multi-antenna heterogeneous cellular networks," *IEEE Trans. Commun.*, vol. 64, no. 7, pp. 3104–3118, July 2016.

[53] G. Geraci, H. S. Dhillon, J. G. Andrews, J. Yuan, and I. B. Collings, "Physical layer security in downlink multi-antenna cellular networks," *IEEE Trans. Commun.*, vol. 62, no. 6, pp. 2006–2021, June 2014.

[54] A. Shojaeifard, K.-K. Wong, W. Yu, G. Zheng, and J. Tang, "Full-duplex cloud radio access network: Stochastic design and analysis," *arXiv:1711.02026*, 2017.

[55] F. Faá di Bruno, "Théorie des formes binaires," *Librairie Breno, Turin.*, 1876.

[56] S. Akbar, Y. Deng, A. Nallanathan, M. Elkashlan, and G. K. Karagiannidi, "Massive multiuser MIMO in heterogeneous cellular networks with full duplex small cells," *IEEE Trans. Commun.*, vol. 65, no. 11, pp. 4704–4719, Nov. 2017.

[57] J. Bai and A. Sabharwal, "Asymptotic analysis of MIMO multi-cell full-duplex networks," *IEEE Trans. Wireless Commun.*, vol. 16, no. 4, pp. 2168–2180, Apr. 2017.

[58] M. Haenggi, J. G. Andrews, F. Baccelli, O. Dousse, and M. Franceschetti, "Stochastic geometry and random graphs for the analysis and design of wireless networks," *IEEE J. Sel. Areas Commun.*, vol. 27, no. 7, pp. 1029–1046, Sept. 2009.

[59] M. Haenggi, *Stochastic geometry for wireless networks*. Cambridge University Press, 2012.

[60] A. Shojaeifard, K. A. Hamdi, E. Alsusa, D. K. C. So, and J. Tang, "Exact SINR statistics in the presence of heterogeneous interferers," *IEEE Trans. Inf. Theory*, vol. 61, no. 12, pp. 6759–6773, Dec. 2015.